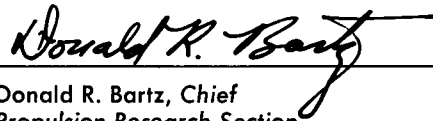Technical Report No. 32-305

Chlorine Trifluoride–Hydrazine Liquid Propellant Evaluation and Rocket Motor Development

Walter B. Powell

James P. Irving

Merle E. Guenther

jpl

JET PROPULSION LABORATORY

CALIFORNIA INSTITUTE OF TECHNOLOGY

PASADENA, CALIFORNIA

May 15, 1963

Chlorine Trifluoride–Hydrazine Liquid Propellant Evaluation and Rocket Motor Development

Walter B. Powell

James P. Irving

Merle E. Guenther

Donald R. Bartz

Donald R. Bartz, Chief
Propulsion Research Section

CONTENTS

TABLES

FIGURES

FIGURES (Cont'd)

ABSTRACT

The chlorine trifluoride–hydrazine liquid bipropellant combination is storable and hypergolic; it has a high average density and gives a moderately high specific impulse. During an experimental program at the Jet Propulsion Laboratory this propellant was handled and used for rocket motor firings. A multi-element "cup and plug" injector was developed which gave good performance and had a reasonable lifetime when used with this propellant. Heat-transfer-rate profile in the chamber and nozzle were determined calorimetrically from tests of a water-cooled sectional rocket motor. Chamber heat transfer determined by the thermocouple-plug transient-temperature measurement method was in good agreement with the calorimetric data. The chlorine trifluoride–hydrazine propellant can be recommended where high density and good performance are required, and for application where short-duration uncooled motors are appropriate.

I. INTRODUCTION

The chlorine trifluoride–hydrazine liquid bipropellant combination is storable and hypergolic; it has a high average density and gives moderately high specific impulse. Because of these desirable features of the ClF_3-N_2H_4 propellant system and its potential usefulness for specialized propulsion applications, an experimental program involving rocket motor firings was conducted by the Jet Propulsion Laboratory. The primary objectives of this program were:

1. To develop equipment and technique for handling ClF_3

2. To develop injectors capable of operating with ClF_3 and yielding satisfactory performance and combustion stability, using uncooled motors and short-duration tests

3. To develop cooled injectors and measure heat-transfer rates, using a water-cooled sectional combustion chamber and nozzle.

Rocket motors and associated equipment have been constructed and operated with ClF_3-N_2H_4, and performance and heat-transfer data have been obtained. An effective exhaust velocity of approximately 7580 ft/sec (for expansion from 300 to 13.5 psia with a nozzle divergence half-angle of 15 deg) is representative of the performance obtained. The heat flux in a 1.67 contraction area ratio chamber at 300 psi chamber pressure was 5.0 to 7.0 Btu/in²-sec, while the maximum heat flux in the nozzle section just upstream of the throat was 7.7 to 10.0 Btu/in²-sec.

II. CHARACTERISTICS OF THE CHLORINE TRIFLUORIDE–HYDRAZINE PROPELLANT SYSTEM

Chlorine trifluoride (ClF_3) as the oxidizer with hydrazine (N_2H_4) as the fuel forms a storable hypergolic liquid bipropellant system. The calculated performance (ideal thermodynamic equilibrium and isentropic flow through a one-dimensional nozzle) for expansion from 300-psia chamber pressure to 14.7-psia exit pressure is given in Table 1. The performance of the ClF_3-N_2H_4 propellant ($c \cong 8300$ ft/sec at $r = 2.2$ to 2.6) is only slightly better than that of the N_2O_4-N_2H_4 propellant ($c \cong 8250$ ft/sec at $r = 1.0$ to 1.2). However, the high specific gravity of ClF_3 (1.80 vs. 1.40 for N_2O_4) and the higher mixture ratio at which the ClF_3 system operates gives the ClF_3-N_2H_4 system a significant advantage in average specific gravity (1.45 at $r = 2.4$ vs 1.17 at $r = 1.1$, respectively) over the N_2O_4-N_2H_4 system.

The vapor pressure of chlorine trifluoride is 17.2 psia at 60°F and rises to 85.6 psia at 140°F. A propellant is considered storable when the tank feed pressure is higher than vapor pressure corresponding to the maximum storage temperature; thus, most pressure-fed chlorine trifluoride–hydrazine rocket motor propulsion systems will be storable.

A hypergolic, storable, high-density, moderately high performance propellant, such as ClF_3-N_2H_4, is particularly well adapted to, and should be considered for, such applications as shipboard or air-launched missiles, storable, instantly ready, defensive missiles, and propulsion systems designed to fire after a long period of coasting in space.

There are certain disadvantages of the ClF_3-N_2H_4 propellant which may limit its usefulness and applicability. The chlorine trifluoride itself is a toxic and extremely active chemical. Chlorine trifluoride has a low upper limit of heat flux in nucleate boiling (Ref. 1), and therefore a limited regenerative cooling capacity. The hydrazine, while itself a good coolant, is present in such small quantity when used with ClF_3 at the mixture ratio for maximum performance that it too has an extremely limited regenerative cooling capacity. These regenerative cooling deficiencies may limit the use of the ClF_3-N_2H_4 propellant to those applications where uncooled or ablative cooled motors are applicable, or where special cooling techniques (such as film cooling) are employed.

Table 1. Chlorine trifluoride–hydrazine. Ideal thermodynamic equilibrium and isentropic flow through a one-dimensional nozzle[a]

r	Location	T, °R	pc/p	A/At	V, ft/sec	Mol. wt.	Cp, cal/mole of total products	γ	CF	Isp, lbf sec/lbm	ρ, lb/ft³	Entropy, cal/°K × mole of fuel	Enthalpy, cal/mole of fuel
1.6	chamber	5857	1.0	∞	0	19.816	8.7	1.297	0	0	0.0946	231.8	−12681.8
	throat	5331	1.8	1.00	4029	20.005	8.7	1.298	1.2443	227.46	0.0587	231.8	−27695.3
	exit	3215	20.4	3.34	8197	20.274	8.2	1.322	1.3938	254.81	0.0086	231.8	−74839.2
2.0	chamber	6267	1.0	∞	0	21.091	8.6	1.300	0	0	0.0941	255.4	−18851.6
	throat	5762	1.8	1.00	4022	21.353	8.6	1.299	1.2419	228.73	0.0583	255.4	−36119.4
	exit	3672	20.4	3.46	8304	21.901	8.3	1.314	1.4015	258.12	0.0082	255.4	−92449.7
2.3	chamber	6499	1.0	∞	0	21.892	8.5	1.303	0	0	0.0942	272.7	−23483.1
	throat	6001	1.8	1.00	4013	22.194	8.6	1.302	1.2410	228.90	0.0584	272.7	−42391.1
	exit	3972	20.4	3.55	8343	22.969	8.4	1.309	1.4060	259.34	0.0079	272.7	−105208.4
2.6	chamber	6675	1.0	∞	0	22.585	8.5	1.307	0	0	0.0946	289.7	−28107.4
	throat	6181	1.8	1.00	3999	22.913	8.5	1.305	1.2403	228.58	0.0586	289.7	−48595.4
	exit	4221	20.4	3.62	8358	23.901	8.5	1.307	1.4097	259.81	0.0078	289.7	−117580.0
2.9	chamber	6793	1.0	∞	0	23.181	8.4	1.311	0	0	0.0954	306.3	−32739.5
	throat	6299	1.8	1.00	3982	23.521	8.4	1.308	1.2400	227.74	0.0591	306.3	−54739.8
	exit	4365	20.4	3.65	8339	24.628	8.4	1.308	1.4114	259.22	0.0077	306.3	−129229.9

Mole fraction of products of combustion

r	Location	N, moles product / moles fuel	H2	H	HF	F2	F	HCl	Cl2	Cl	NH3	N2	N
1.6	chamber	4.205	0.2024	0.0321	0.3951	0.0000	0.0006	0.1192	0.0000	0.0127	0.0000	0.2378	0.0000
	throat	4.165	0.2084	0.0188	0.3993	0.0000	0.0002	0.1254	0.0000	0.0077	0.0000	0.2401	0.0000
	exit	4.110	0.2167	0.0001	0.4049	0.0000	0.0000	0.1349	0.0000	0.0001	0.0000	0.2433	0.0000
2.0	chamber	4.559	0.1276	0.0446	0.4542	0.0000	0.0021	0.1234	0.0000	0.0286	0.0000	0.2194	0.0000
	throat	4.503	0.1319	0.0301	0.4610	0.0000	0.0009	0.1335	0.0000	0.0205	0.0000	0.2221	0.0000
	exit	4.390	0.1397	0.0008	0.4738	0.0000	0.0000	0.1573	0.0000	0.0007	0.0000	0.2278	0.0000
2.3	chamber	4.831	0.0846	0.0483	0.4907	0.0000	0.0044	0.1198	0.0001	0.0451	0.0000	0.2070	0.0000
	throat	4.765	0.0865	0.0344	0.4998	0.0000	0.0021	0.1322	0.0001	0.0351	0.0000	0.2098	0.0000
	exit	4.604	0.0884	0.0017	0.5195	0.0000	0.0000	0.1707	0.0000	0.0024	0.0000	0.2172	0.0000
2.6	chamber	5.108	0.0522	0.0464	0.5211	0.0000	0.0082	0.1112	0.0001	0.0650	0.0000	0.1957	0.0001
	throat	5.035	0.0517	0.0338	0.5327	0.0000	0.0044	0.1246	0.0001	0.0542	0.0000	0.1986	0.0000
	exit	4.827	0.0434	0.0025	0.5601	0.0000	0.0000	0.1792	0.0000	0.0075	0.0000	0.2072	0.0000
2.9	chamber	5.392	0.0292	0.0396	0.5452	0.0000	0.0142	0.0985	0.0002	0.0875	0.0000	0.1854	0.0001
	throat	5.314	0.0269	0.0283	0.5595	0.0000	0.0081	0.1111	0.0002	0.0777	0.0000	0.1882	0.0000
	exit	5.075	0.0089	0.0017	0.5941	0.0000	0.0002	0.1745	0.0001	0.0234	0.0000	0.1970	0.0000

a p_c = 300 psia
p_e = 14.7 psia
Heat of formation of ClF_3 = 44.5 kcal/mole

III. PROPERTIES AND HANDLING OF CHLORINE TRIFLUORIDE

Chlorine trifluoride is an extremely active and toxic chemical. Its physical properties, the materials which can be used with it, and the safe methods of handling it are summarized in the bulletin by the manufacturer (Ref. 2). The density, viscosity, and vapor pressure of chlorine trifluoride were used in reducing the test data reported herein. The values used, given in Table 2 and Fig. 1 and 2, were obtained from Ref. 2. Table 2 and Fig. 3 and 4 give these same properties of hydrazine.

Table 2. Viscosity of μ

Tempera-ture, °F	Viscosity of ClF$_3$ oxidizer[a]		Viscosity of N$_2$H$_4$ fuel[b]	
	centipoises	lb-sec/ft.^{2}	centipoises	lb-sec/ft.^{2}
55	0.4727	9.8726×10^{-6}	1.075	2.2452×10^{-5}
56	0.4695	9.8058×10^{-6}	1.066	2.2264×10^{-5}
57	0.4663	9.7389×10^{-6}	1.058	2.2097×10^{-5}
58	0.4638	9.6867×10^{-6}	1.050	2.1930×10^{-5}
59	0.4604	9.6157×10^{-6}	1.041	2.1742×10^{-5}
60	0.4571	9.5468×10^{-6}	1.033	2.1575×10^{-5}
61	0.4541	9.5841×10^{-6}	1.025	2.1408×10^{-5}
62	0.4515	9.4298×10^{-6}	1.017	2.1241×10^{-5}
63	0.4495	9.3880×10^{-6}	1.010	2.1094×10^{-5}
64	0.4460	9.3150×10^{-6}	1.002	2.0927×10^{-5}
65	0.4430	9.2523×10^{-6}	0.994	2.0760×10^{-5}
66	0.4400	9.1896×10^{-6}	0.986	2.0593×10^{-5}
67	0.4375	9.1374×10^{-6}	0.979	2.0447×10^{-5}
68	0.4350	9.0852×10^{-6}	0.972	2.0301×10^{-5}
69	0.4325	9.0330×10^{-6}	0.965	2.0155×10^{-5}
70	0.4300	8.9808×10^{-6}	0.957	1.9988×10^{-5}
71	0.4270	8.9181×10^{-6}	0.949	1.9820×10^{-5}
72	0.4248	8.8722×10^{-6}	0.942	1.9674×10^{-5}
73	0.4222	8.8179×10^{-6}	0.935	1.9528×10^{-5}
74	0.4198	8.7678×10^{-6}	0.928	1.9382×10^{-3}
75	0.4170	8.7093×10^{-6}	0.921	1.9236×10^{-5}
76	0.4145	8.6570×10^{-6}	0.914	1.9089×10^{-5}
77	0.4120	8.6048×10^{-6}	0.907	1.8943×10^{-5}
78	0.4095	8.5526×10^{-6}	0.899	1.8776×10^{-5}
79	0.4073	8.5067×10^{-6}	0.892	1.8630×10^{-5}
80	0.4048	8.4545×10^{-6}	0.886	1.8505×10^{-5}
81	0.4022	8.4002×10^{-6}	0.879	1.8358×10^{-5}
82	0.4000	8.3542×10^{-6}	0.872	1.8212×10^{-5}
83	0.3976	8.3041×10^{-6}	0.865	1.8066×10^{-5}
84	0.3954	8.2581×10^{-6}	0.859	1.7941×10^{-5}
85	0.3930	8.2080×10^{-6}	0.853	1.7815×10^{-5}
86	0.3905	8.1558×10^{-6}	0.846	1.7669×10^{-5}
87	0.3882	8.1078×10^{-6}	0.840	1.7544×10^{-5}
88	0.3859	8.0597×10^{-6}	0.834	1.7418×10^{-5}
89	0.3837	8.0138×10^{-6}	0.828	1.7293×10^{-5}
90	0.3812	7.9616×10^{-6}	0.822	1.7168×10^{-5}

a "Chlorine Trifluoride and Other Halogen Fluorides", Technical Bulletin TA8532-2, General Chemical Div., Allied Chemical Co., New York, N. Y.
b "Anhydrous Hydrazine", Olin Mathieson Chemical Corp., Baltimore, Md.
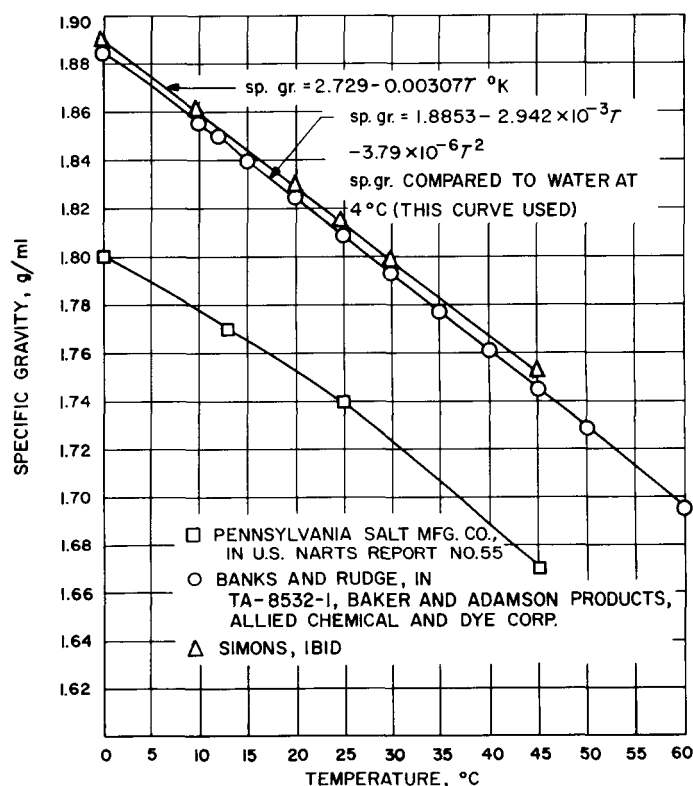
Fig. 1. Specific gravity of liquid chlorine trifluoride

Chlorine trifluoride, though extremely active, does not attack copper, brass, steel, monel, nickel, or aluminum due to the formation of a passive metal fluoride film which protects the metal from further corrosion. The anhydrous material is shipped in mild steel cylinders. Propellant tanks and lines of the test stand installation were made of 18-8 stainless steel, type 347 or 304ELC where welding was required, and type 303 for machined parts. Type 6061 aluminum alloy was used for aluminum-brazed injector assemblies, for welded aluminum parts and chamber sections, and for motor mounting brackets. Soft aluminum (2S-0) or soft copper were used as gaskets in serrated flange joints.

All of the materials mentioned above and used in the test program will react with chlorine trifluoride if sufficient activation energy is supplied, or if the ignition temperature is exceeded. Chlorine trifluoride reacts spontaneously at room temperature with water or ice and with most hydrocarbons and oxidizable substances. Reaction with impurities or contaminants in a system can

pressure, where it is allowed to remain for several minutes.

Passivation as described above may burn off small amounts of residual contaminants at a slow rate, so that any heat liberated can be dissipated without raising adjacent material to its ignition temperature. Its most important function, however, is to form a passive fluoride film on all exposed surfaces. This film protects the surface from further attack.

Chlorine trifluoride piping must be both clean and tight. Connections should be welded where possible. Permanent joints made up with threaded parts should be back-brazed or silver soldered. Where a threaded joint must be assembled so that it can be taken apart, Teflon tape wrapped around the male fitting, starting a few threads back from the entering end, is helpful in assur-
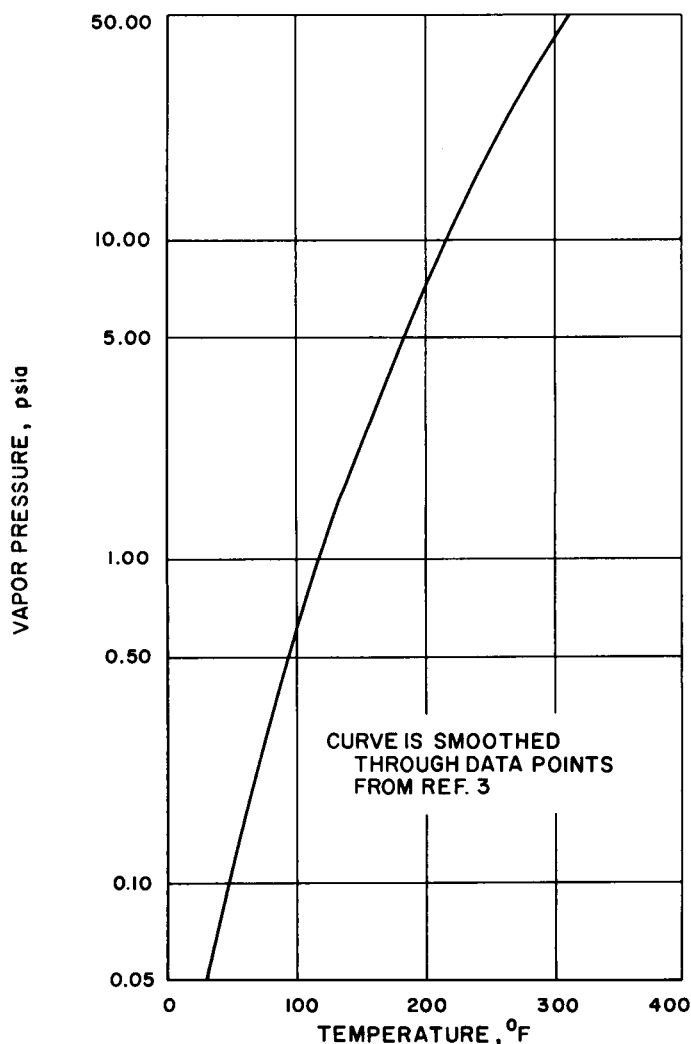
Fig. 5. Results of Teflon–chlorine trifluoride reaction bomb tests

ing a leak-tight joint. Alternatively, Teflon emulsion can be brushed on the threads and the assembly can be completed after air-drying. Connections that are to be opened regularly can be made with flanged, gasketed type fittings, or with the AND standard flared tube fittings.

Because of its extreme toxicity, chlorine trifluoride must be handled with caution. Chlorine trifluoride was used at one test stand at the JPL test station at Edwards Air Force Base for over three years without any incidents involving personnel. All operations with ClF_3 were performed remotely, with one exception—the making of connections between the test-stand tank-filling lines and the one-ton cargo vessels in which the material was received. Here the manual valve was opened under ambient vapor pressure by an operator wearing full protective clothing and standing behind a protective shield. A similarly clothed operator stood nearby, and a third man watched from a distance. This operation is shown in Fig. 6. No personnel were ever exposed to equipment containing ClF_3 at higher than ambient vapor pressure.

The protective clothing mentioned above was made from a Teflon cloth coated with Kel-F elastomer. With it was used an aluminum hard-hat having an acetate face shield and a Teflon cloth drape over the back of the neck. Hysol synthetic rubber gloves and Neoprene rubber boots were also worn as part of the ensemble. Operations on components and lines that had been emptied, vented, and purged with nitrogen were performed by two operators wearing conventional acetate face shields and the Hysol synthetic rubber gloves.

Fig. 4. Vapor pressure of anhydrous hydrazine
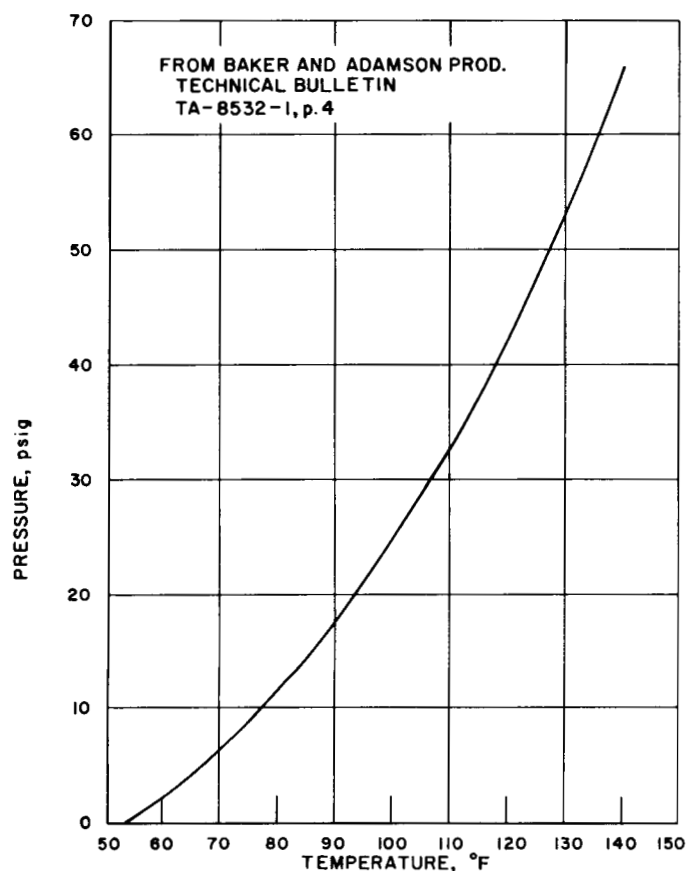
Fig. 2. Vapor pressure of liquid chlorine trifluoride

Fig. 3. Density of anhydrous hydrazine

cause local hot spots which can initiate combustion of ClF_3 and the primary system.

Teflon is believed to be the only plastic material which can be used in contact with chlorine trifluoride. In compatibility tests conducted at JPL a thin film of grease, or even absorbed water, was sufficient to cause ignition and destruction of Teflon specimens. Clean Teflon, on the other hand, is not affected by chlorine trifluoride at temperatures below approximately 300°F and can be used for both static and dynamic seals. Ref. 4 reports a series of tests made at JPL in which a ball valve having perfectly clean Teflon seals was used to shut off a ClF_3 stream moving at 35 ft/sec, and was then cycled many times in quiescent ClF_3 at 500-psi pressure. No deterioration of the Teflon seals was noted. As part of the same investigation specimens of perfectly clean Teflon were immersed in ClF_3 in a clean "bomb" and subjected to various conditions of pressure and temperature, and a locus of reaction conditions was determined. In all the tests there were no failures of clean Teflon in the pressure and temperature region below the curve of Fig. 5, either in static bomb tests or in a flow system.

It is important that all ClF_3 equipment be cleaned thoroughly to remove grease, scale, pipe dope, paint, moisture, and other contaminants. Cleaning involves three steps:

1. Removal of all obvious foreign matter by mechanical means, pickling, and washing.

2. Flushing with a nonaqueous cleaning and preliminary drying solvent such as acetone or trichloroethylene, followed by a thorough purging with dry nitrogen.

3. Passivation with chlorine trifluoride by slowly displacing the nitrogen gas in the system with chlorine trifluoride vapor at atmospheric pressure; closing the system vent when the displacement is complete; and raising the ClF_3 pressure *slowly* to the working

IV. TEST STAND INSTALLATION AND OPERATION

The test stand used for the ClF_3-N_2H_4 rocket motor tests was an open structure located on the JPL test facility at the Edwards Air Force Base. Figure 7 is a side view of the stand showing the tankage and the test motor mounting. The large tank at the forward end of the stand contains water used for cooling. The two upper tanks behind the water tank are used for the fuel, hydrazine. The two tanks in the lower cell are used for the oxidizer, chlorine trifluoride. An uncooled rocket motor is mounted at the forward end of a massive concrete block, and is fired downward at an angle toward a deflector plate at the bottom of a shallow trench. The motor is mounted on a thrust bed which is supported by flexure members and restrained in the thrust direction by a load cell.

data. Auxiliary purge, bleed, and vent lines, water coolant circuits, control circuits, and operational instrumentation are not shown. Heat-transfer data were obtained by a transient-temperature-measurement technique with the uncooled motors, and from calorimetric measurements when sectional water-cooled motors were used. The equipment and instrumentation used for heat-transfer determinations are described more fully in Sect. VIII.

Fig. 7. Side view of test stand showing tankage and test motor mounting
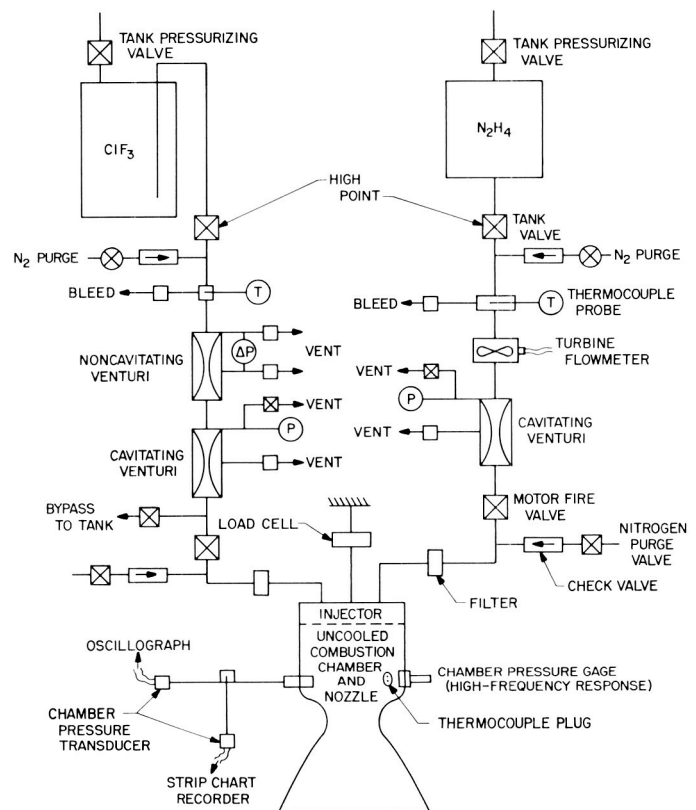
Fig. 8. Simplified circuit diagram of ClF_3-N_2H_4 test setup

The simplified circuit diagram (Fig. 8) shows the primary propellant lines and controls and the primary instrumentation used to obtain the desired performance

A simple nitrogen gas pressurized propellant feed system was used for the motor tests. Flow in the fuel circuit was measured with a turbine meter and with a cavitating venturi. The turbine meter was located upstream of the cavitating venturi, with a length of straight pipe between the two meters sufficient to ensure undisturbed flow at the entrance to the venturi. Flow in the oxidizer circuit was measured with a noncavitating venturi and a cavitating venturi in series. The two venturis were separated by a length of straight pipe, and the noncavitating venturi was placed in the upstream position because it was
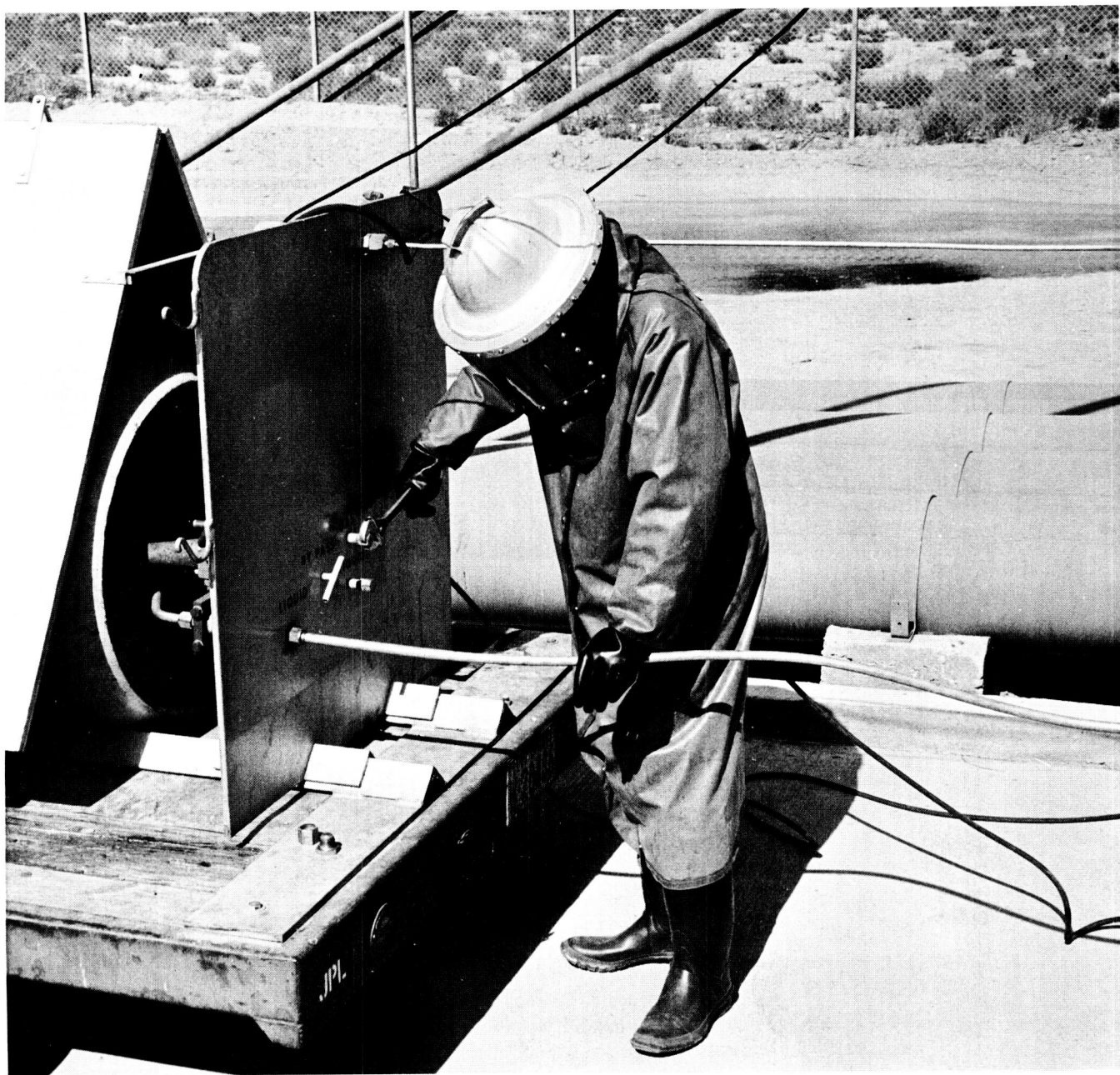
Fig. 6. Operator wearing full protective clothing while making connection to ClF₃ supply cylinder

Chlorine trifluoride was vented from the test-stand area through a vertical line extending above the rest of the test-stand installation. Operations involving venting of ClF₃ were carried on only when a steady breeze was blowing from the west, so that fumes were carried away from the other test station operating areas. The test stand had been located originally to take advantage of a prevailing westerly wind.

No personnel were allowed to work in an area where the odor of chlorine trifluoride was objectionable, and exposure with any perceptible odor was kept as short as possible.

ignition problem was solved by introducing a nitrogen purge flow into the lines immediately downstream of the fire valves before and during the start. This nitrogen purge was supplied at a pressure lower than propellant feed pressure and entered through a check valve, so that it was automatically cut off as the propellant line pressure approached steady-state value. The pressure built up in the injector manifold by the nitrogen purge reduced the possible compression pressure ratio and the resultant heating, so that no further trouble was experienced with the filters in the lines between the fire valves and the injector.

The starting transient, as it was experienced in the final system, was as follows: From the instant the valves started to open to the time that steady-state combustion was established was approximately 0.3 to 0.5 sec. This time was about equally divided between filling the lines and injector manifold and the gradual rise of pressure in the combustion chamber.

not likely to introduce flow disturbances which could affect a downstream meter. The cavitating venturis were always used in the downstream location because of the possibility that bubbles of vapor or previously dissolved gas might persist for some distance and interfere with the operation of a downstream flowmeter.

A turbine flowmeter was used in the ClF_3 circuit during a portion of the test program. Rulon, an impregnated Teflon, seemed to be the best of several materials tried as bearings for the rotor shaft. However, even with the Rulon bushings installed, the turbine meter had to be disassembled, rinsed, and dried after each day's testing to prevent buildup of deposits in the bearings and consequent loss of calibration due to friction. Use of turbine flowmeters in the ClF_3 circuit was discontinued after one of the meters was destroyed in a fire. The second of two consecutive tests had been shut down for several seconds, with the propellant tanks and lines still pressurized, when ignition occurred suddenly and unexpectedly in the region of the turbine meter, probably starting at a completely contained Teflon gasket used to seal the joint between the flare tube end on the turbine meter and the mating fitting on the propellant line. This was the only unexplained incident involving ClF_3 which was experienced during the entire test program.

An apparent interaction between the rocket motor and the flow measurement system was detected and corrected during the period of investigation. It was noted that the series flowmeters in each propellant circuit were not agreeing with each other; the cavitating venturi would indicate a flow rate 2 to 3% higher than that indicated by the corresponding turbine meter or noncavitating venturi, although the pressure levels were such that cavitation would seem to be assured.

During the period when the flow-rate discrepancies were being experienced, a motor with a 12- to 13-in.-long combustion chamber was being used. This motor operated with a clearly audible "scream" of approximately 1000- to 1300-cycle/sec frequency, apparently corresponding to the first longitudinal mode of the combustion chamber. When the combustion chamber length was reduced to 8 in., the scream was absent from the motor noise. Coincident with this change, the series flowmeters began to indicate flow rates which differed by less than 1%. This correlation seemed to indicate that the effect of the chamber pressure fluctuation peaks had extended up the propellant lines and had been able to modify the flow through the cavitating venturi.

Because of the uncertainty in the flow-rate measurements obtained during screaming motor operations, the fact that screaming operation may also affect the general performance level and the heat transfer, and because screaming is not the intended or desirable mode of operation, performance and heat transfer are reported herein only for the final series of tests where relatively stable combustion was obtained and flow-rate measurements were in agreement. These stable tests were made using a motor with an 8-in.-long cylindrical chamber section and a 14-element injector (the motor and injector configuration will be described in detail in Sect. V). The several other injectors that were tested earlier in the program performed unsatisfactorily in that combustion was rough, performance was obviously low, or there was localized erosion of the injector or the chamber, indicating nonuniform mixture and velocity distributions within the combustion chamber. These injectors are described in Appendix A.

Two procedures which were used in ensuring prompt, smooth starts of the short-duration uncooled motor tests should be discussed in connection with the simplified circuit diagram (Fig. 8). It was found necessary to purge the propellant lines between the tanks and the motor starting valves of all traces of residual gas; otherwise, the initial flow and combustion was extremely rough. The propellant lines were purged in the following manner: The fuel tank valve was opened and fuel under hydrostatic head was bled through manually operated valves from the pressure pick-up lines at the entrance and throat of the venturi and at the high point of the slightly sloping line just downstream of the fuel tank valve; this was done before the tank was pressurized. The oxidizer tank valve was opened and oxidizer was allowed to flow through the line and out a bypass valve near the motor valve into the smaller of the two oxidizer tanks. In addition the oxidizer was bled from the pressure pick-up lines at the inlet and throat of each venturi and from the high point of the slightly sloping line just downstream of the tank valve. Oxidizer bleeding was done after the tank was pressurized, and the valves were all remotely operated.

The motors were started by opening the oxidizer and fuel fire valves, admitting propellants to the injector and quickly establishing equilibrium combustion conditions. The sudden admission of propellant compressed the air in the line between the valve and the injector orifices, resulting in a temperature increase which, in one instance, was sufficient to cause ClF_3 to react with a filter screen which was built into an injector. This compression-

V. ROCKET MOTOR AND INJECTOR CONFIGURATIONS TESTED

Two types of motors and several injector configurations were used during the test program. Each injector was evaluated in a series of short-duration tests using a heavy-weight uncooled combustion chamber and nozzle assembly. After an injector having satisfactory characteristics had been developed, a sectional-cooled combustion chamber was available to make longer test firings, so that injector cooling and durability could be demonstrated and chamber and nozzle heat-transfer distribution data could be obtained. The cooled-motor tests were made only with the one injector configuration which gave satisfactory over-all performance. With these tests, the program was terminated.

The uncooled motor assembly is shown in Fig. 9. The combustion chamber, including the 2-in. instrumentation section, is made of mild steel and has a $5/8$-in.-thick wall. The throat section of the two-piece exhaust nozzle is made of high-purity copper and is chrome-plated on the inside surface. The motor shown is the final configuration, with a cylindrical combustion chamber 5 in. in diameter and 8 in. long. The exhaust nozzle has a throat diameter of 3.90 in. and an exit diameter of 7.50 in. The chamber area ratio Ac/At is thus 1.65, a rather low value, which means that chamber gas velocities and pressure drops were relatively high. The exit area ratio Ae/At is 3.72, which is approximately correct for expansion of the 300 psia chamber pressure gases to a one-atmosphere exit pressure.

The 2-in. instrumentation section is shown in detail in Fig. 9. It is a replaceable chamber section which carries the various chamber pressure taps. In all instances this section was installed at the downstream end of the chamber, immediately upstream of the nozzle entrance, where the combustion was most nearly complete and the products of combustion most nearly uniformly distributed. The high-frequency-response chamber-pressure transducer tap shown accommodated a water-cooled Photocon Model 345[1] transducer in an adapter (not shown) so that the sensing diaphragm was isolated from the surface of the combustion chamber by a passage $1/8$-in. in diameter and 1 in. long. The adapter was found necessary to protect the Photocon transducer diaphragm from burnout, but it also had the effect of reducing drastically the maximum frequency for flat response of the combined assem-

bly over that for a flush-mounted Photocon transducer. The low-frequency response chamber-pressure tap line was branched to connect to two Taber[2] transducers.

Thermocouple plugs, used in determining heat transfer to the uncooled motors, were installed in the instrumentation sections of the chamber for some tests. Fig. 9 shows one type of thermocouple plug used. The thermocouple plugs and the method of obtaining the heat-transfer rate from the temperature data are described in detail in Sect. VIII of this Report.

The injector, the mounting flange (which becomes an integral part of the combustion chamber), the combustion chamber sections, and the exhaust nozzle are held together firmly by spring-loaded bolts, with the joints between sections sealed by Durabla or soft aluminum gaskets.

The sectional cooled combustion chamber and nozzle which were used for the final series of tests are shown in Fig. 10. The cooled adapter flange was made of aluminum alloy. The chamber sections had stainless steel outer rings, with the coolant passage inner shell either of copper 0.060-in. thick, silver soldered in place, or of stainless steel 0.040-in. thick, heliarc-welded to the outer ring. The exhaust nozzle inner liner, with its coolant passage separating rings, was machined from one piece of copper, and the three-piece-split stainless-steel outer shell was bolted together around it. The nozzle, the chamber sections, adapter flange, and injector were held together by through-bolts, as with the uncooled motor assembly, except that in this case no spring-loading was used. The joints were all sealed with O-rings to prevent leakage. Each section of the chamber and nozzle was cooled by a separately metered flow of water. Chamber pressure of the cooled motor was measured through an internal passage in a chamber section outer ring which opened into the region between the inside of the combustion chamber and O-ring seal. The frequency response capability of such a pressure tap is extremely limited. It was not possible to incorporate a tap for a high-frequency response pressure transducer into the cooled-motor assembly, so no such pressure records were obtained with that motor. The size and shape of the combustion chamber and nozzle of the cooled motor was identical to that

---

[1]Photocon Research Products, Pasadena, Calif.

[2]Taber Instruments Co., North Tonawanda, N. Y.
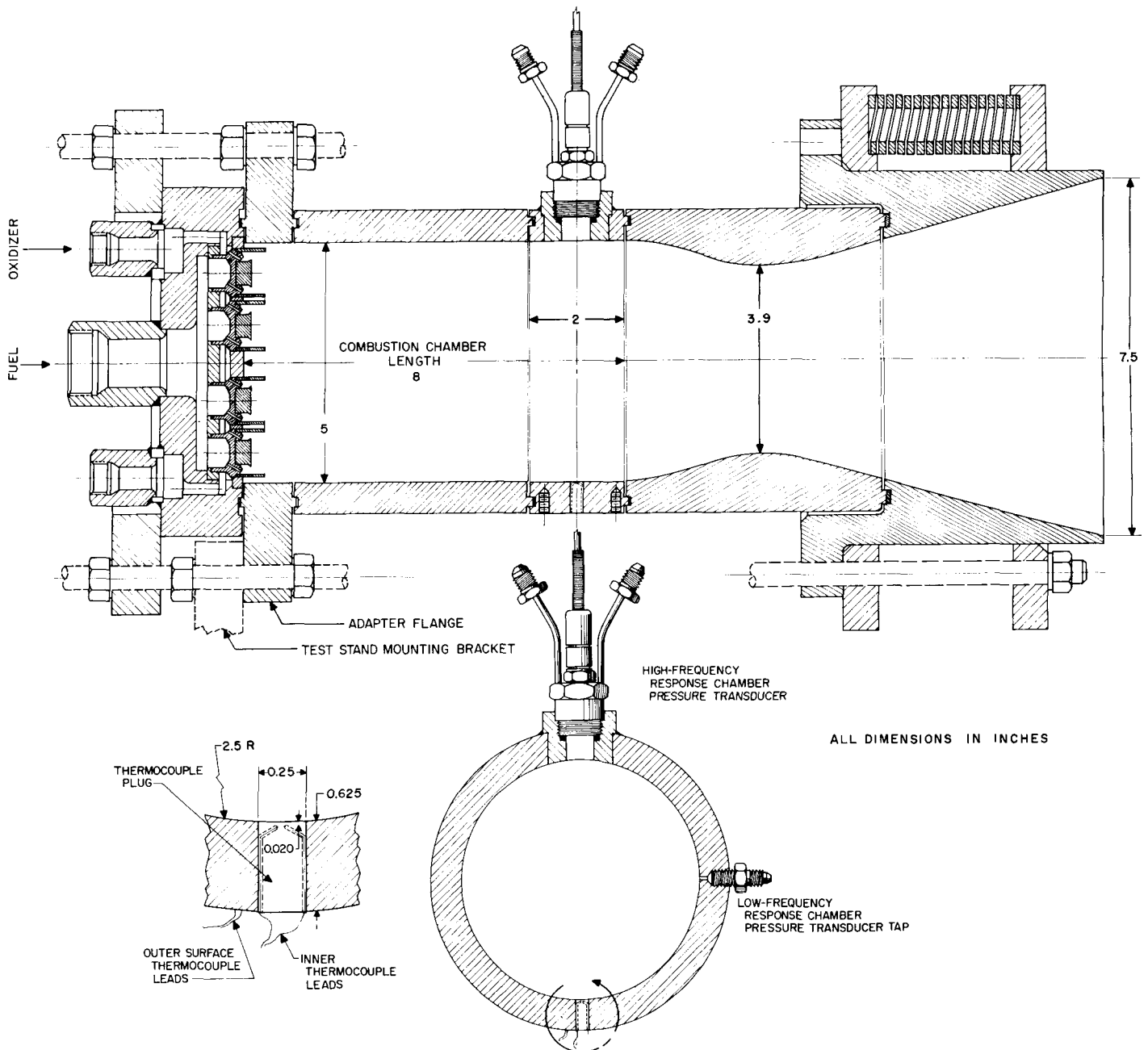
Fig. 9. Uncooled thrust chamber assembly

of the uncooled motor, except that the exhaust nozzle was expanded to an exit area ratio of $\epsilon = 3.86$.

The modified showerhead multi-element cup-and-plug injector shown in Fig. 9 and 10 was used for the final series of tests in which the performance and heat-transfer data presented in Sect. VII and VIII of this report were obtained. This injector configuration was preceded by a series of injectors, described briefly in the Appendix,

which were unsatisfactory for a variety of reasons. Most of the injector problems were associated with the extreme reactivity of the chlorine trifluoride. A misdirected stream of oxidizer or reacting propellant mixture, or a recirculating eddy of hot combustion gases, could quickly erode the metal of an injector or combustion chamber, be it copper, aluminum, or stainless steel. Other injector configurations tested gave rough, irregular combustion or poor performance.
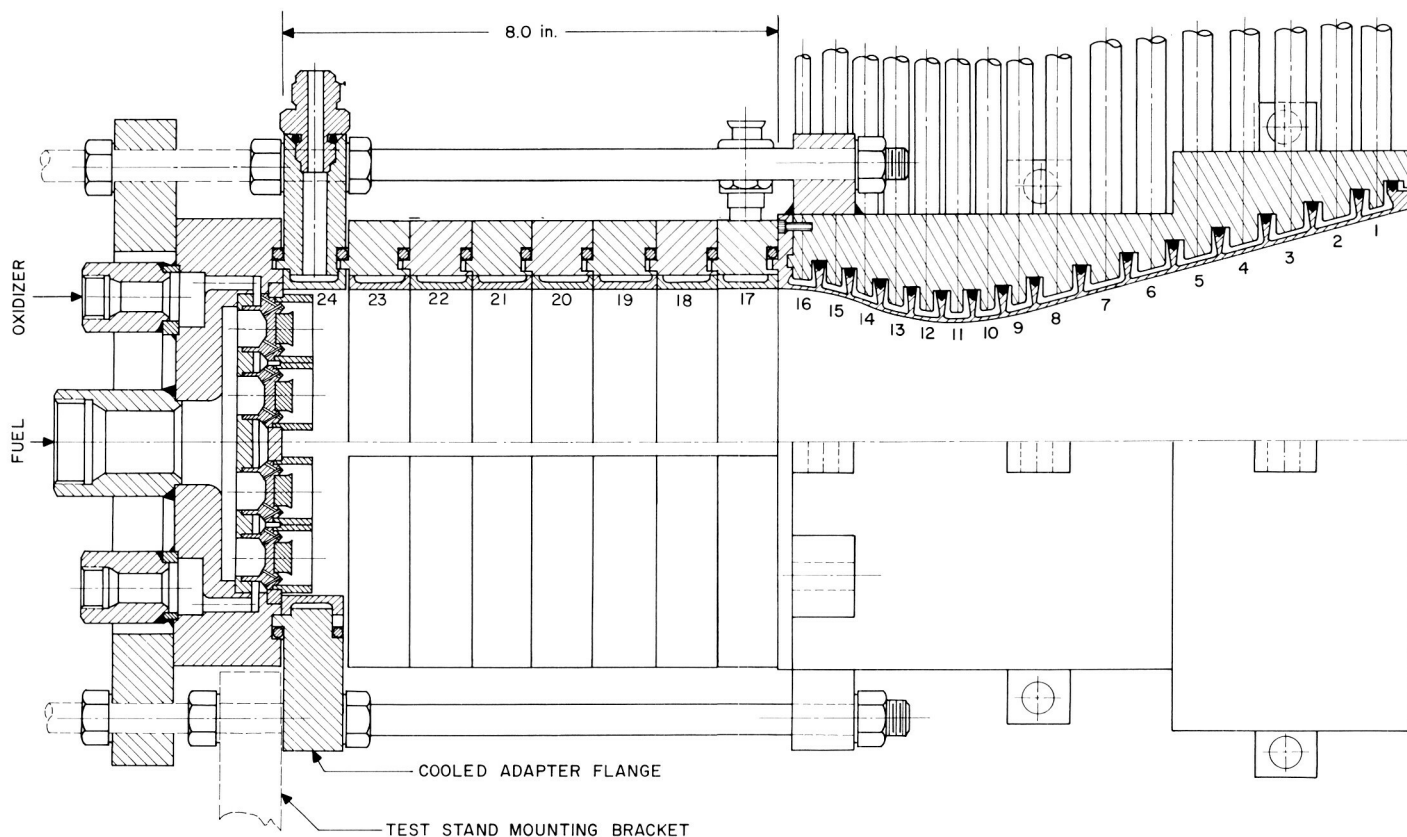
Fig. 10. Sectional water-cooled thrust chamber assembly

The injector shown in Fig. 9 and 10 was developed to meet, as far as possible, the following list of desirable attributes:

1. Uniform distribution of propellant across combustion chamber cross section

2. Good mixing of propellants and uniform mixture-ratio distribution

3. Longitudinal distribution of atomization, evaporation, and mixing of the incoming propellant

4. Protection of initial mixing region from transverse pressure waves

5. Near-axial momentum of discharged propellant

6. Cooling and protection from erosion of injector parts

7. Simple fabrication, with subassemblies which can be inspected before final assembly

The multi-element cup and plug injector shown in Fig. 9 and 10 and illustrated in Fig. 11 approached the

above requirements by using 14 cup-and-plug injector elements, each 1 in. in diameter, distributed across the face of the injector. Each element had 12 orifices for each propellant, so that propellant distribution and gross
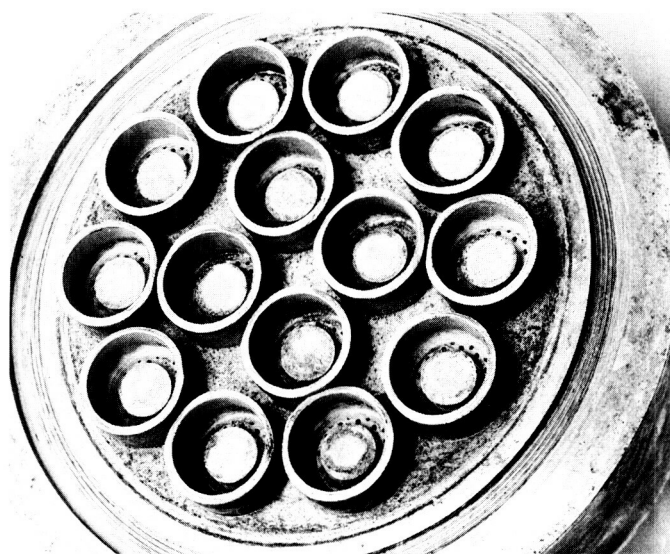
Fig. 11. Multi-element cup-and-plug injector face

mixture-ratio uniformity were satisfactory. The orifices in the injector elements were sized so that at an operating mixture ratio of $r = 2.2$, the nominal velocities of the chlorine trifluoride and hydrazine propellant streams were 90 to 100 ft/sec. The oxidizer streams from the base of the injector element were directed inward, so that they impinged on and spread out over the surface of the central plug; in spreading out, the edges of the adjacent oxidizer sheets collided and an outwardly deflected radial sheet, or rib, was also formed. Thus, the oxidizer came off the central plug in the form of a thin, cylindrical sheet with outwardly projecting, radial ribs. The fuel streams were similarly directed toward the inside surface of the cup, and the fuel issued from the cup in the form of a cylindrical sheet with inwardly projecting radial ribs. The oxidizer and fuel orifices were spaced in between each other in the base. The propellant thus issued from each injector element in the form of two concentric, cylindrical, thin sheets with alternate radial ribs of each propellant extending toward the cylinder of the opposite propellant, as idealized in Fig. 12. The plug was completely blanketed with oxidizer, and the cup was protected with a layer of fuel, except where some of the oxidizer rib spray splashed against the cylinder wall near the open end. Thus, the injector parts were cooled and protected by the unmixed propellant components.

The cup extended beyond the top of the plug by an amount called the "cup length," creating a protected volume in which mixing and reaction could occur. While there was some mixing of stray spray of propellant within the cup and some mixing by intersection of ribs with cylindrical sheet flow, both within and outside the cup, most of the propellant mixing was by evaporation and mass transfer between the adjacent thin sheets of propellant as they traveled down the chamber. This mixing process is similar to that of a conventional shower-head injector, except that it should be accelerated due to the increased surface area of the propellant sheets over that of undeflected streams. Since the mixing process was distributed in the direction of the axis of the combustion chamber, the amplification of longitudinal pressure waves in the combustion chamber through interaction with the combustion process should be minimized. Because the elements were closely and as uniformly spaced as possible on the injector face plate, there was no tendency to create powerful recirculating currents of hot gas which could erode the chamber walls. At the same time, the many small recirculating currents of hot gas generated in the spaces between the moving propellant sheets promoted evaporation, mass transfer, mixing, and re-action of the propellant components. The cups shielded the sheet formation and the initial mixing within each element from disturbing influences, such as radial or tangential-mode pressure waves. The cups also assured that the propellant was discharged in a predominantly axial direction with no misdirected streams which could strike and erode a chamber wall.

The cup-and-plug injector was made entirely of aluminum alloy, and the separate parts were assembled in one aluminum brazing operation, except for the welding of the back manifold cover ring and the inlet fittings. This method of assembly made it possible to fabricate an injector having a large number of small propellant orifices, yet in which the holes were drilled in groups in separate subassemblies which could be inspected before the final assembly.

Application of the principles of propellant injection and mixing and of fabrication discussed above resulted in an injector which gave good performance and had a satisfactory lifetime when used with the chlorine trifluoride–hydrazine propellant. Their application to other propellants and injector problems may be profitable.
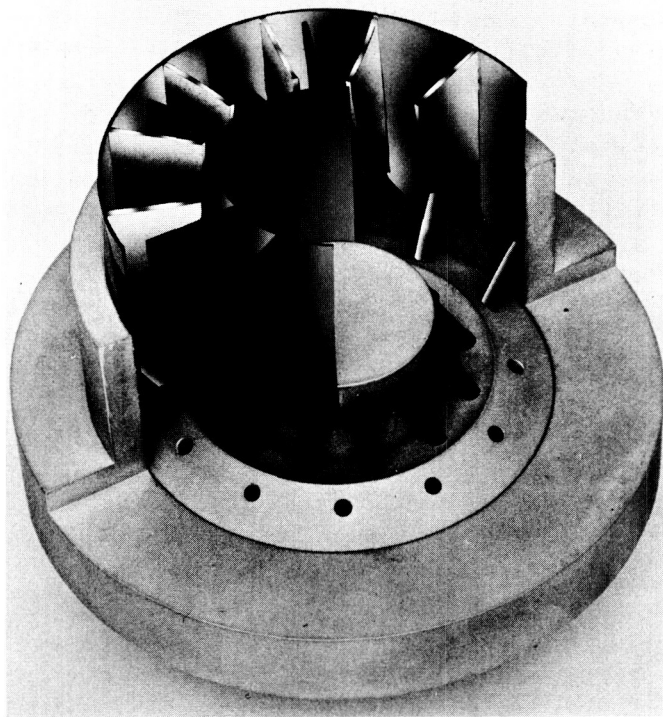

Fig. 12. Idealized distribution of propellant leaving injector element

VI. INSTRUMENTATION AND PERFORMANCE CALCULATIONS

The circuit diagram (Fig. 8) shows the basic instrumentation which was used to obtain the data required to compute the performance achieved during each test.

The oxidizer flow was measured with a noncavitating venturi and with a cavitating venturi, in series. Each venturi was equipped with an upstream and a throat pressure tap, and the temperature of the fluid was measured in the line upstream of the venturis.

The fuel flow was measured with a turbine flowmeter, downstream of which was a cavitating venturi having an upstream and a throat pressure tap. Fuel temperature was measured in the line upstream of the flowmeters.

The venturis were calibrated by water flow tests and the over-all flow coefficient,[3] $C' = w/[\gamma(p_{up} - p_t)]^{1/2}$, was determined as a function of the upstream flow Reynolds number, $Re = w/(\pi/4)d\,\mu$. The physical properties of the propellants required for computing the flow rates are given in Fig. 1, 2, 3, and 4 and in Table 2. The difference between upstream and throat pressures of the noncavitating venturis was measured directly with a Foxboro[4] differential pressure transducer, chosen because it could withstand the required case pressure and, in the case of the chlorine trifluoride, because the strain-sensitive wire elements of the transducer were completely isolated from the working fluid. For the cavitating venturis, the upstream pressure was measured directly and the throat pressure was taken as the saturation pressure corresponding to the measured upstream propellant temperature. An attempt was made to measure the cavitating venturi throat pressure directly but lack of suitable low-range differential pressure gauges, and the time required for the pressure tap collection manifold and line to reach equilibrium pressure under cavitating conditions, prevented useful data from being obtained.

The rotation speed of the turbine in the turbine flowmeter in the fuel line was measured either by a direct count of revolutions against a time base, or as an integrated rate signal from a Waugh[5] converter; both methods gave the same rate. Volume flow rate as a function of turbine rotational speed was based on a water calibration and fuel-weight-flow rate was computed by multiplying the indicated volume flow rate by the density of the fuel.

The combustion chamber pressure was measured just upstream of the entrance to the nozzle through taps installed in motor sections, as previously described. The pressure records used in computing propellant and motor performance were obtained using a Taber pressure transducer, which was connected to the pressure tap by a short length of ⅛-in. D tubing. The output of this transducer was recorded on a strip chart recorder. The output of a second Taber transducer connected to the same chamber pressure tap was recorded on a C.E.C.[6] oscillograph tape along with a time base and other records of thrust, valve-operation sequence, etc. Because of the small connecting lines, the Taber transducer pressure systems had a linear frequency response up to only approximately 10 cycle/sec. These transducers were calibrated against a dead-weight tester.

The high-frequency-response pressure transducer tap on the uncooled motor chamber instrumentation section was fitted with a Photocon Model 345 pressure transducer mounted in a protective adapter so that the pressure reached the transducer diaphragm through a passage ⅛-in. in diameter and 1 in. long. As discussed previously, the adapter was required to protect the transducer diaphragm from the burnouts which were experienced when a flush installation was used. As a consequence of the protective adapter, however, the natural frequency of the system was reduced to approximately 2100 cycles/sec, and the damping was such that the response amplitude ratio was up 10% at 600 cycle/sec and up 30% at 1000 cycle/sec. These characteristics were determined from shock-tube tests using a duplicate of the tap configuration. Because of these limitations no really high-frequency response data could be obtained. The output of the Photocon transducer was recorded on magnetic tape, from which it could be transcribed to an oscillograph chart or processed through a frequency analyzer.

The test motor was mounted on a frame which was suspended from a rigid support by interconnecting flexure members. Motion in the direction of the thrust axis was restrained by a strain-gauge-type load cell. Calibrating loads for this thrust-measuring system were applied

---

[3]See Nomenclature
[4]The Foxboro Co., Foxboro, Mass.
[5]Waugh Engineering Co., Van Nuys, Calif.

---

[6]Consolidated Electrodynamics Corp., Pasadena, Calif.

by a pneumatic cylinder acting through an identical load cell which had been calibrated at the Bureau of Standards. The propellant lines leading to the motor were deliberately made nonrigid so as to have little effect on the motion of the thrust stand, and any remaining elastic restraint due to the connecting lines was included in the over-all thrust calibration.

The throat area of the rocket motor nozzle was computed from measurements of the throat diameter made before and after each test. Combustion chamber inside diameter was 5 in. for all tests. The nominal combustion chamber area ratio was 1.65, and exhaust nozzle exit area ratio was 3.72 for the uncooled nozzle and 3.86 for the cooled nozzle.

Rocket motor and propellant performance is customarily evaluated by computing the effective exhaust velocity, the characteristic velocity, and the thrust coefficient from the experimental data and comparing these values with corresponding data of other experimenters and with results of thermodynamic calculations based on ideal combustion and isentropic equilibrium expansion of the combustion products through a one-dimensional nozzle. Thus

$$c_{eff} = \frac{Fg}{w}$$

$$c^* = \frac{p_c A_t g}{w}$$

$$C_F = \frac{F}{p_c A_t}$$

and

$$c_{eff} = c_{th} x_1$$

$$c^* = c^*_{th} x_2$$

$$C_F = C_{Fth} x_3$$

where the factors x_1, x_2, and x_3, account for imperfect combustion, shift of equilibrium, loss of heat to chamber walls or coolant, nozzle curvature, boundary layer and nonuniform velocity distribution effects, and nozzle exit divergence angle.

The correction factors indicated above generally differ from unity by only a few percent.

The chamber pressure appearing in the performance parameter calculations is the isentropic stagnation pressure at the throat of the nozzle. For the case of the cylindrical combustion chamber with propellant introduced at one end, reaction with heat addition occurring within the chamber, and constant composition isentropic expansion through a nozzle, the relation between isentropic stagnation pressure at the nozzle throat and the static pressure at the upstream and downstream ends of

the cylindrical combustion chamber can be calculated. The generalized results of such a set of calculations are shown in Fig. 13. The present series of tests were made with a chamber-to-nozzle throat area ratio of $A_c/A_t = 1.65$, and, assuming the ratio of specific heats of the combustion gases to be $\gamma = 1.30$, the ratio of static pressure at the downstream end of the combustion chamber to the isentropic stagnation pressure at the nozzle throat is $p_2/p_c = 0.905$. This ratio was used in computing the effective chamber pressure used in tabulating and plotting the performance data.
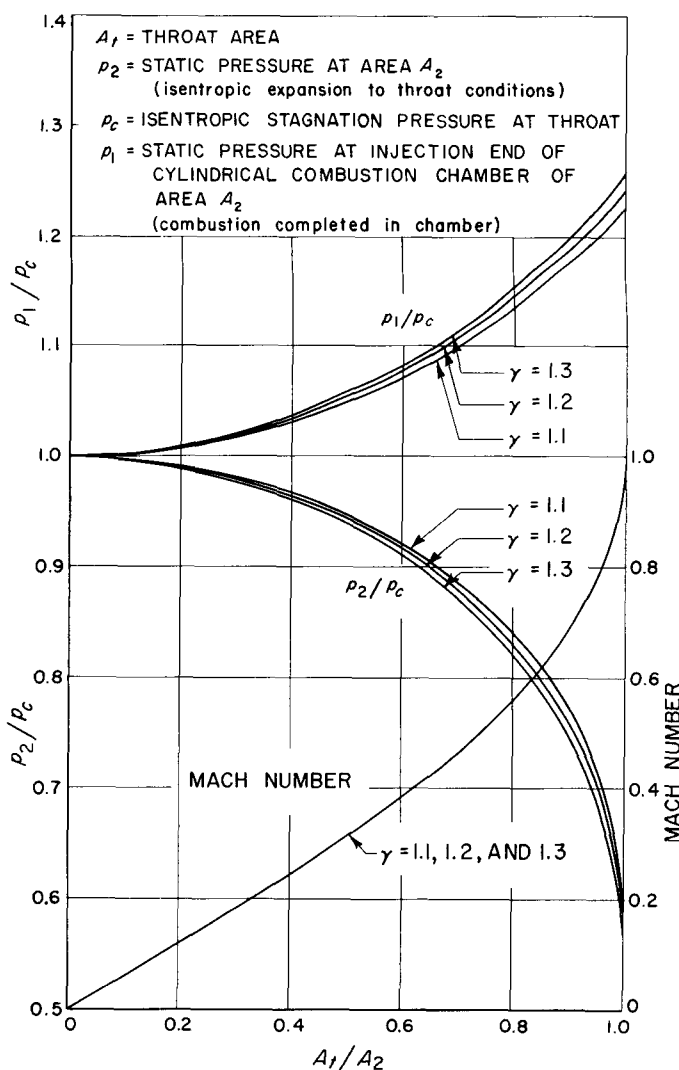

Fig. 13. Chamber pressure ratio and Mach number vs. area ratio for cylindrical combustion chamber

The effective chamber pressure obtained in the manner described above was not deemed accurate enough to be used in computing the experimental performance

parameters c^* and C_F. The ideal system correction of almost 10% is derived with the assumptions of a non-reacting gas and of no heat transfer through the nozzle walls. Actual conditions during the test program differed from these assumptions, with a resulting effect of unknown magnitude on the correction factor. Had the area ratio of the combustion chamber A_c/A_t been higher, the chamber-static-pressure/throat-stagnation-pressure ratio would have been closer to one, and uncertainty in the value of this correction ratio would have had less effect on the computed value of the effective chamber pressure. This points out a disadvantage associated with

using motors having low values of the chamber area ratio A_c/A_t for experimental investigations of propellants. Rather than compute values of characteristic velocity and thrust coefficient which would be in error by an unknown amount, it was decided to evaluate the performance of the propellant and motor in terms of the effective exhaust velocity, which could be computed from the measured propellant flow rates and the thrust without the use of any approximate correction factors. All performance results presented in this report are thus in terms of effective exhaust velocity, propellant mixture ratio, and approximate effective chamber pressure.

VII. PERFORMANCE OBTAINED

The data obtained from the tests made with the final injector configuration, and after the combustion-chamber length had been decreased to eliminate scream, are given in Table 3. The effective exhaust velocity obtained from the reduction of the experimental data is plotted on Fig. 14. Also shown on Fig. 14 is the calculated exhaust velocity for the propellant (from Table 1). The calculated exhaust velocity is for ideal expansion from 300 psia to 14.7 psia, while the experimental data was obtained at approximately 300 psia chamber pressure and with 13.5 psia external pressure. The effect of this decrease in external pressure at near-optimum nozzle exit area ratio is to increase the effective exhaust velocity by approximately 1%; therefore, the proper theoretical exhaust velocity for comparison with the experimental data is 1% higher than the calculated values shown for reference on Fig. 14.

The effective exhaust velocity obtained with modified showerhead multi-element cup-and-plug injectors having

a cup length of 0.40 and 0.42-in. was between 7380 ft/sec and 7720 ft/sec over a mixture ratio range of $r = 1.7$ to 2.4, with most of the tests falling in the range of $c_{eff} = 7580 \pm 80$ ft/sec. When the cups were cut back to give a cup length of 0.32-in. and then 0.25-in., there was a decrease in performance of approximately 150 ft/sec.

At a mixture ratio of $r = 2.1$ the corrected calculated exhaust velocity for thermodynamic equilibrium and isentropic expansion from 300 psia to 13.5 psia through a one-dimensional nozzle is $c_{th} = 8400$ ft/sec. The average experimental effective velocity of $c_{eff} = 7580$ ft/sec is 9.8% less than this calculated value. Of this difference, 1½% can be ascribed to axial momentum loss due to divergence of the exhaust jet, 1¼% may be due to heat loss in the chamber nozzle, either absorbed in the walls during the short-duration tests of the uncooled motors or transferred to the coolant water during the longer tests of the cooled motor. This leaves a 7.1% performance

Table 3. Test data from a multi-element cup-and-plug injector

Test No.	$r = \dfrac{w_o}{w_f}$	$P_{c,\,eff}$, psia	$c_{,\,eff}$, ft/sec	Motor assembly[a]	Injector	Temperature probe	Chamber heat-flux $q_{max} =$ Btu/in.²-sec	Wall temperature for q_{max}, °F	Notes
253	1.93	300.1	7647	uncooled	No. 2 with 0.40-in. cup length	Thermocouple plug Thermocouple approx. 0.020 in. from inside wall Random alignment with respect to injector cups	7.90	775	New cooled nozzle liner
254	2.21	304.7	7666				7.00	790	
255	2.23	300.9	7598				6.55	890	
256	2.39	304.0	7589				6.55	850	
257	1.73	302.7	7609				6.52	835	
258	1.93	306.8	7723				7.40	790	
259	2.01	292.4	7655	cooled	No. 2 with 0.40-in. cup length				
260	2.23	300.8	7577						
261	2.33	292.4	7399						
262	2.05	298.1	7535	uncooled	No. 2 with 0.40-in. cup length	Surface thermocouple, copper plate, random alignment	4.50	780	
263	2.19	301.9	7506				5.30	790	
264	2.37	301.9	7381				5.00	810	
265	2.21	303.4	7499	cooled	No. 2 with 0.32-in. cup length				Ends of injector cups showing erosion
266	2.07	298.1	7519						
267	1.86	302.1	7538						
268	1.70	302.1	7593						
269	1.72	302.3	7547						
270	1.87	297.7	7515	cooled	No. 2 with 0.32-in. cup length				
271	2.19	293.5	7276						
272	2.41	304.5	7441	uncooled	No. 2 with 0.32-in. cup length	Surface thermocouple nickel plate { In line with injector cups / In between injector cups }	6.95	990	
273	2.04	291.8	7439				—	—	
274	2.37	305.6	7479				5.70	720	
275	2.02	292.2	7405				4.65	780	
276	2.33	309.6	7524	uncooled	No. 2 with 0.25-in. cup length		6.68	725	Replated thermocouple surface
277	2.03	295.9	7448	uncooled	No. 2 with 0.25-in. cup length	Surface thermocouple nickel plate { In line with injector cups / In between injector cups }	6.05	640	
278	2.37	305.3	7430				6.23	735	
279	2.04	292.5	7380				—	—	
280	2.06	292.2	7436				4.95	810	
281	2.39	306.3	7430				5.28	790	
282	2.07	294.2	7578	uncooled	No. 3 with 0.42-in. cup length	Surface thermocouple nickel plate { In line with injector cups / In between injector cups }	6.22	705	New injector
283	2.40	311.1	7660				6.31	790	
284	2.05	295.1	7544				5.86	700	
285	2.40	306.9	7521				5.47	500–800	
286	2.42	305.2	7299	cooled	No. 2 with 0.25-in. cup length				
287	2.02	—	7427						
288	2.04	291.1	7580	cooled	No. 3 with 0.42-in. cup length				25-sec test, nozzle erosion
289	2.35	293.3	7533						
290	2.20	297.7	7652						

a Uncooled motor as in Fig. 9; Cooled motor as in Fig. 10. For all motors: $d_c = 5$ in., $l_c = 8.00$ in., $d_t = 3.90$ in., $\varepsilon = 3.72$ to 3.86, $p_e \cong 13.5$ psia. Injector configuration as in Fig. 9 and 10.
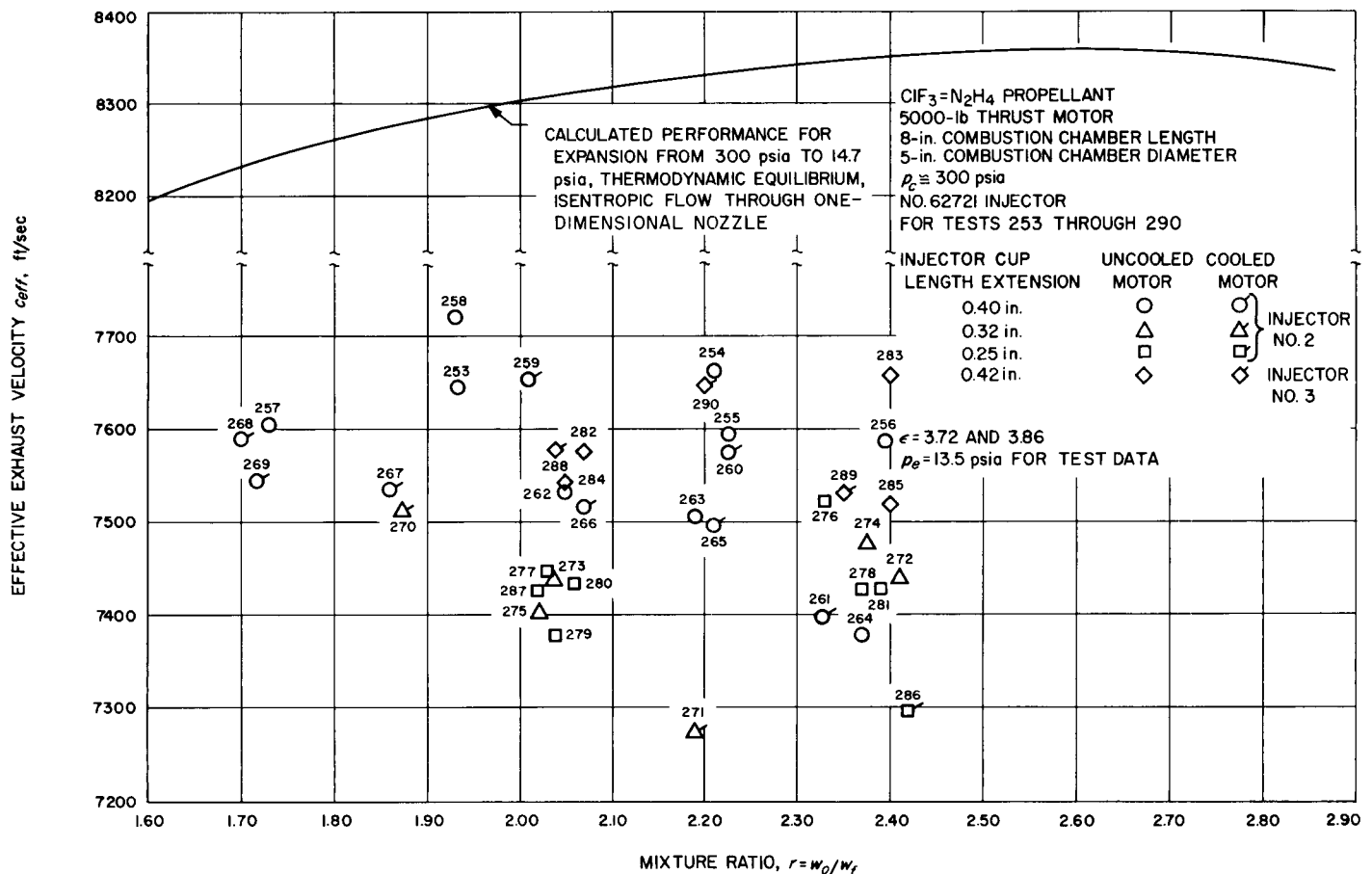
Fig. 14. Effective exhaust velocity obtained with ClF₃-N₂H₄ propellant using cooled and uncooled motors with various injector modifications

deficiency which must be ascribed to incomplete combustion of the propellant. This combustion efficiency of 92.9%, obtained with the injector and combustion chamber described herein, is not as high as might ultimately be obtained, but attempts to increase the performance above this level were thwarted by injector burnout and by the occurrence of combustion instability.

Combustion stability of the ClF₃-N₂H₄ rocket motor using the multi-element cup-and-plug injector and the 8-in. long chamber appeared to be satisfactory from the reports of observers and from analysis of the chamber pressure records. As previously mentioned, the same motor configuration with a 13-in. long chamber section operated with a loud scream which appeared to have a frequency in the neighborhood of the first longitudinal mode frequency of approximately 1300 cycle/sec. This scream was the predominant feature of these tests to the observers, but its frequency was too near to the natural frequency (2100 cycle/sec) of the high-frequency pres-

sure-gauge tap configuration to enable the magnitude of the chamber-pressure perturbations to be deduced from the records. From analysis of shock-tube test data, 600 cycle/sec appeared to be the upper limit of response for the tap configuration if excessive distortion of the amplitude of the signal was to be avoided.

When the motor was assembled with the 8-in. chamber section, the scream disappeared from the combustion noise. Again, this was apparent to the observers. Table 4 shows the pressure perturbations which were measured in the range from 10 to 600 cycle/sec during tests using 13-in. and the 8-in. combustion chamber sections. The measurable perturbations are well within tolerable limits (average pressure of oscillation less than 2.6 psi with chamber pressure of 300 psia). In the frequency range of 1000 to 4000 cycle/sec, where the amplification of the signal would be very high, the average pressure of the disturbances with the 8-in. chamber section was no more than 2.2 psi, while in the same region the amplitude of the disturbances with the 13-in. chamber approached 30

psi. These data support the belief, based primarily on observer reports, that the motor with the 8-in. chamber section operated stably and without excitation of the first longitudinal mode of chamber pressure oscillation.

A further object of the development and test program, besides the achievement of satisfactory performance, was to demonstrate control of the erosive potential of the ClF_3-N_2H_4 propellant in the injector and combustion chamber environment. Both the injector and the water-cooled exhaust nozzle liner were found to have a useful lifetime in service, even though subject to gradual attack and erosion. The ends and inside walls of the cups of the injector were most obviously affected by repeated operation. The No. 2 injector, used for tests 253 through 281 as shown on Table 3, had a total operating time of approximately 100 sec., and the ends of the cups had twice been cut back, when it was finally retired. The No. 3 injector was in good shape after four 1½-sec. tests and two 5-sec. tests, when it was subjected to a final 25-sec. test. At the conclusion of this test, with a total of 41 sec. of operation, the ends of the cups were beginning to show a little erosion (Fig. 11) but there was considerable useful life left in this injector.

The cooled nozzle inner liner was machined of one piece of copper. A clean copper surface, not chrome-plated, was exposed to the combustion gases. A new nozzle inner liner was installed for Test No. 259 and was used for all cooled motor tests for the remainder of the program. This amounted to fourteen 5-sec. tests and the one final 25-sec. test. There was gradual erosion and grooving of the copper surface in the contraction and throat regions of the nozzle as the test series progressed. This attack tended to occur in bands approximately in line with the outer ring of cylindrical elements of the injector, indicating that a reacting mixture, and perhaps some liquid droplets, were entering the nozzle. At the conclusion of the final 25-sec test the throat section of the nozzle was deeply grooved, and there were several small leaks in the nozzle liner. This erosion is shown in Fig. 15. The lifetime of the cooled nozzle was thus between 70 and 95 sec slightly less than that of the injector.

The water-cooled cylindrical combustion chamber sections did not give any problems due to insufficient cooling or to chemical attack or erosion.

These results indicate that the objective of developing a satisfactorily nonerosive ClF_3-N_2H_4 combustion system was partly achieved. The injector, the chamber, and the
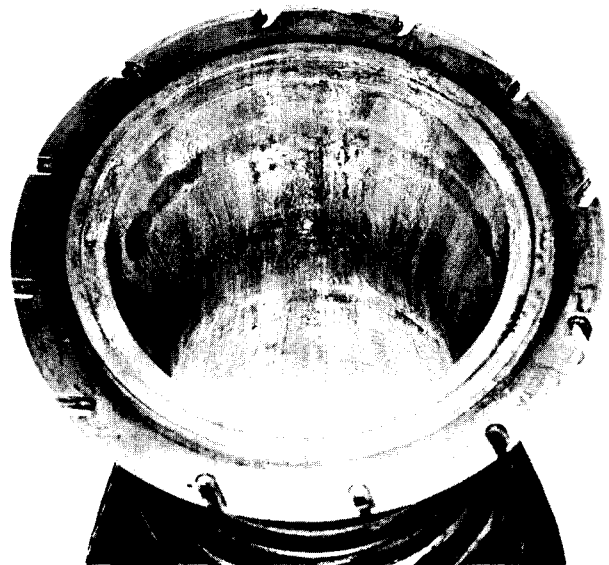

Fig. 15. Entrance section of sectional water-cooled exhaust nozzle, showing erosion streaks in line with outer row of injector elements

nozzle, if adequate cooling was provided, could be operated for periods of approximately one minute. Longer duration operation may be possible if the injector is further developed to improve:

1. The cooling and protection of the element cup

2. The atomization and evaporation of the propellant

Some improvement might also be obtained by increasing the area ratio A_c/A_t of the chamber, so that the velocity of any fluid particles entering the nozzle flow would be decreased.

Table 4. Average pressure of oscillations in various frequency bands with combustion chambers of two different lengths

Frequency band	Average pressure, psi	
	Test 250, $l_c = 13$ in.	Test 254, $l_c = 8$ in.
10–50	0.9	1.9
10–100	1.2	2.6
100–200	0.8	0.4
200–300	0.8	0.2
300–400	0.5	0.1
400–500	0.4	0.1
500–600	0.4	0.2

VIII. HEAT-FLUX MEASUREMENTS

Heat flux can be determined from transient-temperature measurements taken in the metal walls of uncooled rocket motors during short-duration tests, as well as from calorimetric measurements taken during steady-state operation of cooled motors. The transient-temperature measurement technique was used to measure the heat transfer at the downstream end of the cylindrical combustion chamber during tests of the ClF_3-N_2H_4 system using the uncooled rocket motor shown in Fig. 9. During tests using the sectional cooled motor (Fig. 10) a complete profile of the heat transfer in the combustion chamber and nozzle was obtained.

A. Heat Flux From Cooled Motor Tests

For the cooled motor tests, water coolant from a common manifold was supplied to each of the 24 annular coolant passages through individual cavitating venturis sized to give the required coolant flow. Difference thermocouples were used to determine the coolant temperature rise between the supply manifold and the outlet from each coolant passage. Thermocouple outputs were fed into a MicroSADIC[7] system and recorded on a magnetic tape which was used as input to a digital computer programed to give the temperature rise of the water coolant. In addition, the temperature rise data for a few of the coolant passages were recorded independently on a conventional strip chart recorder. Coolant flow rates were determined from the pressure in the water manifold and the calibrations of the individual venturis.

Heat-transfer data were obtained calorimetrically during 14 of the 15 tests made with the water-cooled sectional motor having an 8-in. long chamber. No data were obtained from one test due to instrumentation difficulties. All of these tests were of 5-sec duration except the final test, which was of 25-sec duration. Typical values of average heat flux to each of the separately cooled sections of the chamber and nozzle are shown in Fig. 16 through 23, where the sections are numbered to correspond to the numbers shown in Fig. 10. The liner material of sections 1 through 23 (copper or stainless steel) is identified in Fig. 16 through 23. Section 24, the adapter flange, was aluminum in all tests. In Fig. 16, 17, and 18 the heat-flux increases in the chamber with distance downstream from the injector except that the last cham-
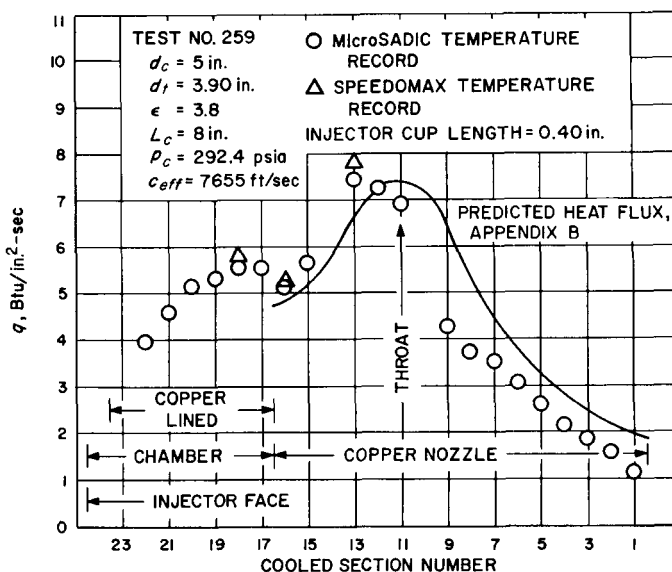

Fig. 16. Experimental heat-flux results obtained with sectional water-cooled thrust chamber assembly using ClF_3-N_2H_4 propellant at $r = 2.01$
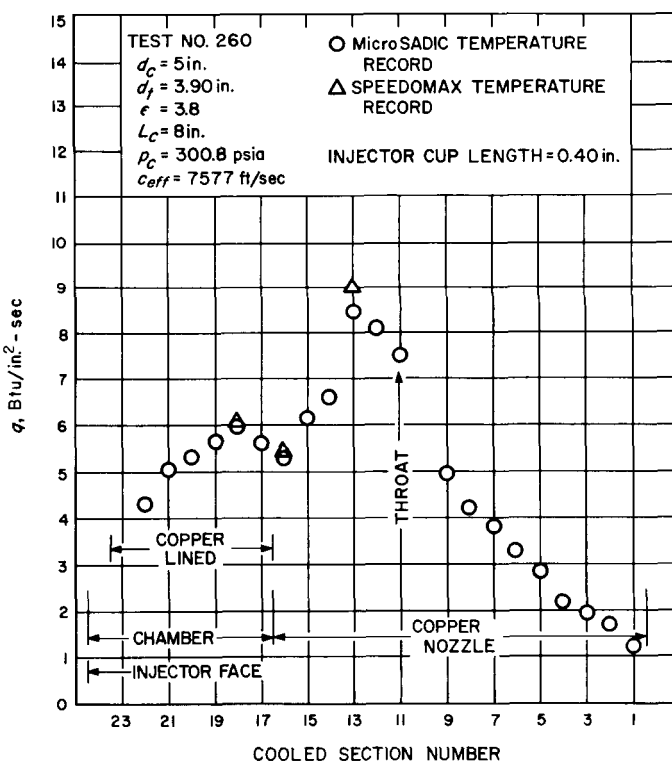

Fig. 17. Experimental heat-flux results obtained with sectional water-cooled thrust chamber assembly using ClF_3-N_2H_4 propellant at $r = 2.23$

---

[7]Consolidated Electrodynamics Corp., Pasadena, Calif.

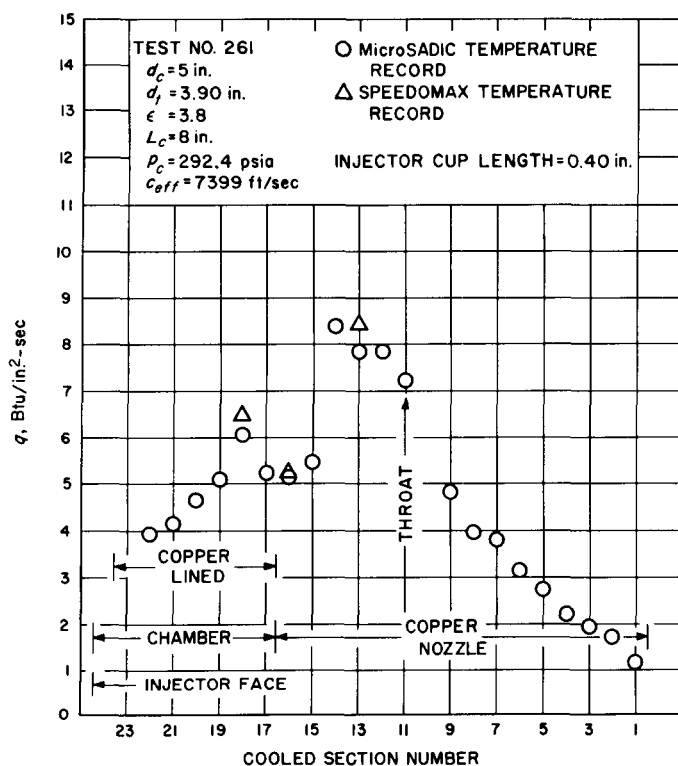**Fig. 18. Experimental heat-flux results obtained with sectional water-cooled thrust chamber assembly using ClF₃-N₂H₄ propellant at $r = 2.33$**

Fig. 19. Experimental heat flux results obtained with sectional water-cooled thrust chamber assembly using ClF₃-N₂H₄ propellant at $r = 1.87$

ber section, immediately upstream of the nozzle converging section, shows a decrease in the heat flux. The maximum heat flux in the chamber varies from 5.6 Btu/in²-sec to a high of 6.5 Btu/in²-sec. The maximum heat flux in the nozzle is 9.0 Btu/in²-sec in the second section upstream from the nozzle throat section. These tests were made using the No. 2 cup and plug injector when it was fairly new and in good condition; the cup length or extension of the cups beyond the tops of the plugs was 0.40-in. The data shown in Fig. 19 and 20 were obtained with the same injector after the cup length had been cut down to 0.32-in.; no appreciable differences in heat-transfer rate or distribution were found. Similar results were obtained when the cup length of this injector was cut down to 0.25-in., although a slight drop in performance was evidenced.

The sectional motor heat-transfer data shown in Fig. 21, 22 and 23 were obtained using the No. 3 cup-and-plug injector, with a cup length of 0.42 in. These data are somewhat incomplete due to several individual thermocouple failures, but again the heat flux in the cylindrical combustion chamber is 5 to 6 Btu/in²-sec. The maximum heat flux, two sections upstream of the throat, is 9 to 10
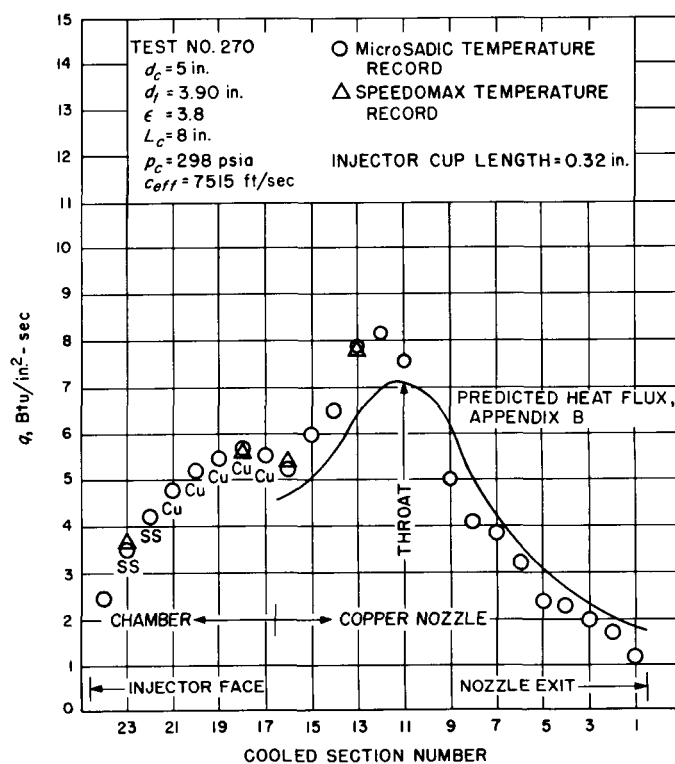
Btu/in.²-sec. The chief difference between the data obtained with this injector and that obtained earlier is that the chamber heat flux is almost constant along its length, rather than being low at the injector end and increasing toward the nozzle end. No reasonable explanation of this minor difference could be found.

Heat-transfer rate is shown as a function of ClF₃-N₂H₄ mixture ratio for various chamber and nozzle sections in Fig. 24, 25, 26 and 27. Figure 24 shows the heat flux to motor section 18, the second chamber section upstream of the nozzle entrance, for all the tests made using the cooled motor and the cup and plug injectors, including those in which the cup length was reduced. Figure 25 shows the heat flux for the same tests at motor section 17, the section immediately upstream of the nozzle. The heat flux in the chamber sections is 5 to 6 Btu/in.²-sec and shows no significant trend with mixture ratio between $r = 1.7$ and 2.4.

The heat flux at motor section 11, the nozzle throat, is shown in Fig. 26. Figure 27 shows the maximum nozzle heat flux, which occurred at the first or second section upstream of the nozzle throat in all tests. The heat flux
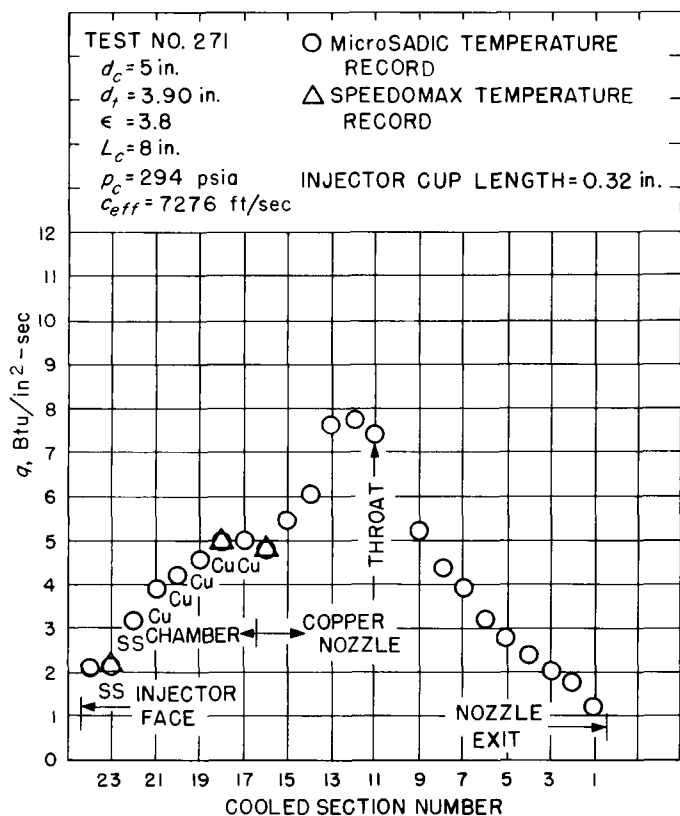
Fig. 20. Experimental heat flux results obtained with sectional water-cooled thrust chamber assembly using CIF_3-N_2H_4 propellant at $r = 2.19$

Fig. 21. Experimental heat flux results obtained with sectional water-cooled thrust chamber assembly using CIF_3-N_2H_4 propellant at $r = 2.04$

Fig. 22. Experimental heat-flux results obtained with sectional water-cooled thrust chamber assembly using ClF_3-N_2H_4 propellant at $r = 2.35$
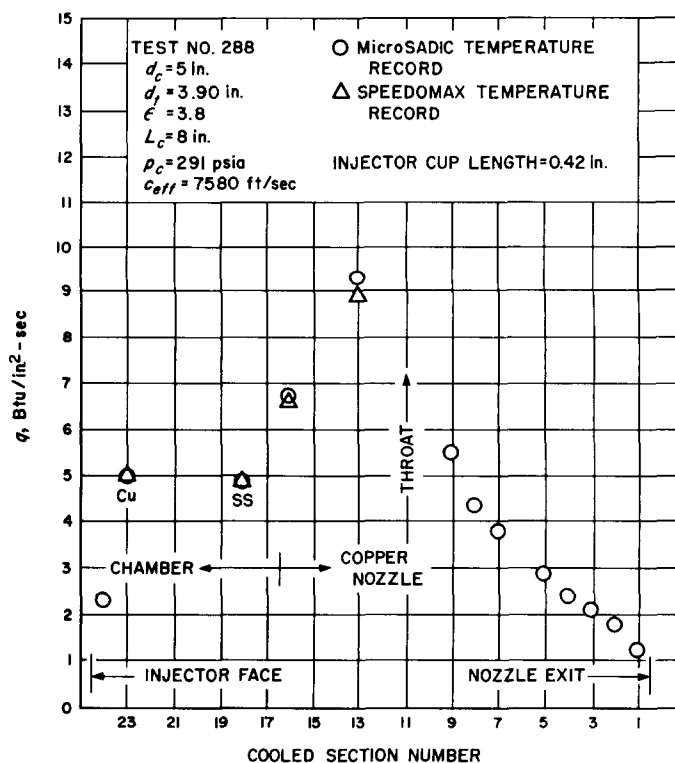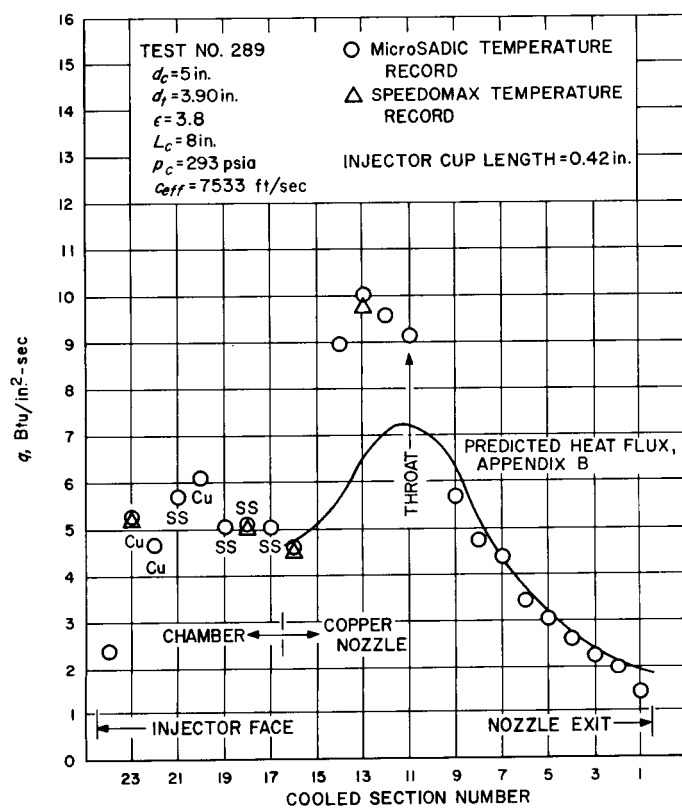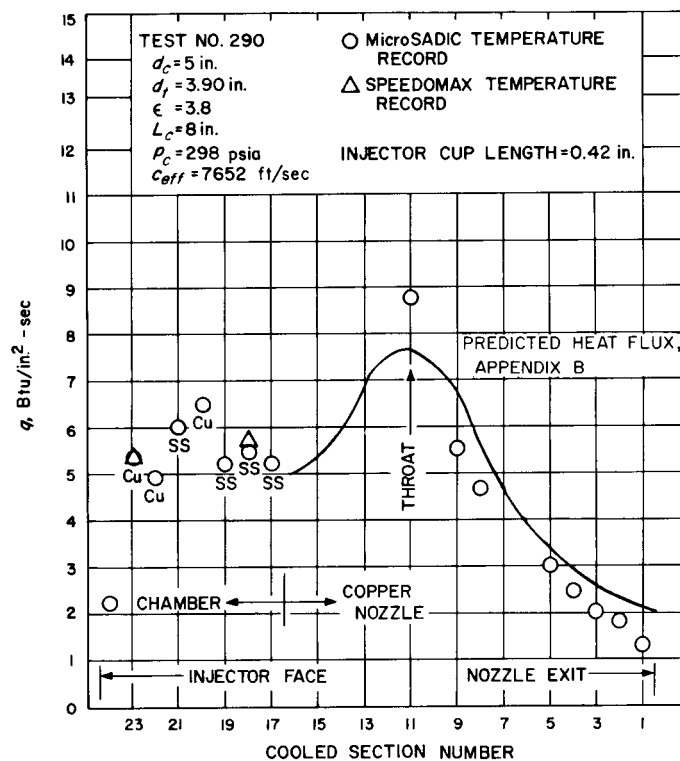

Fig. 23. Experimental heat-flux results obtained with sectional water-cooled thrust chamber assembly using ClF_3-N_2H_4 propellant at $r = 2.20$
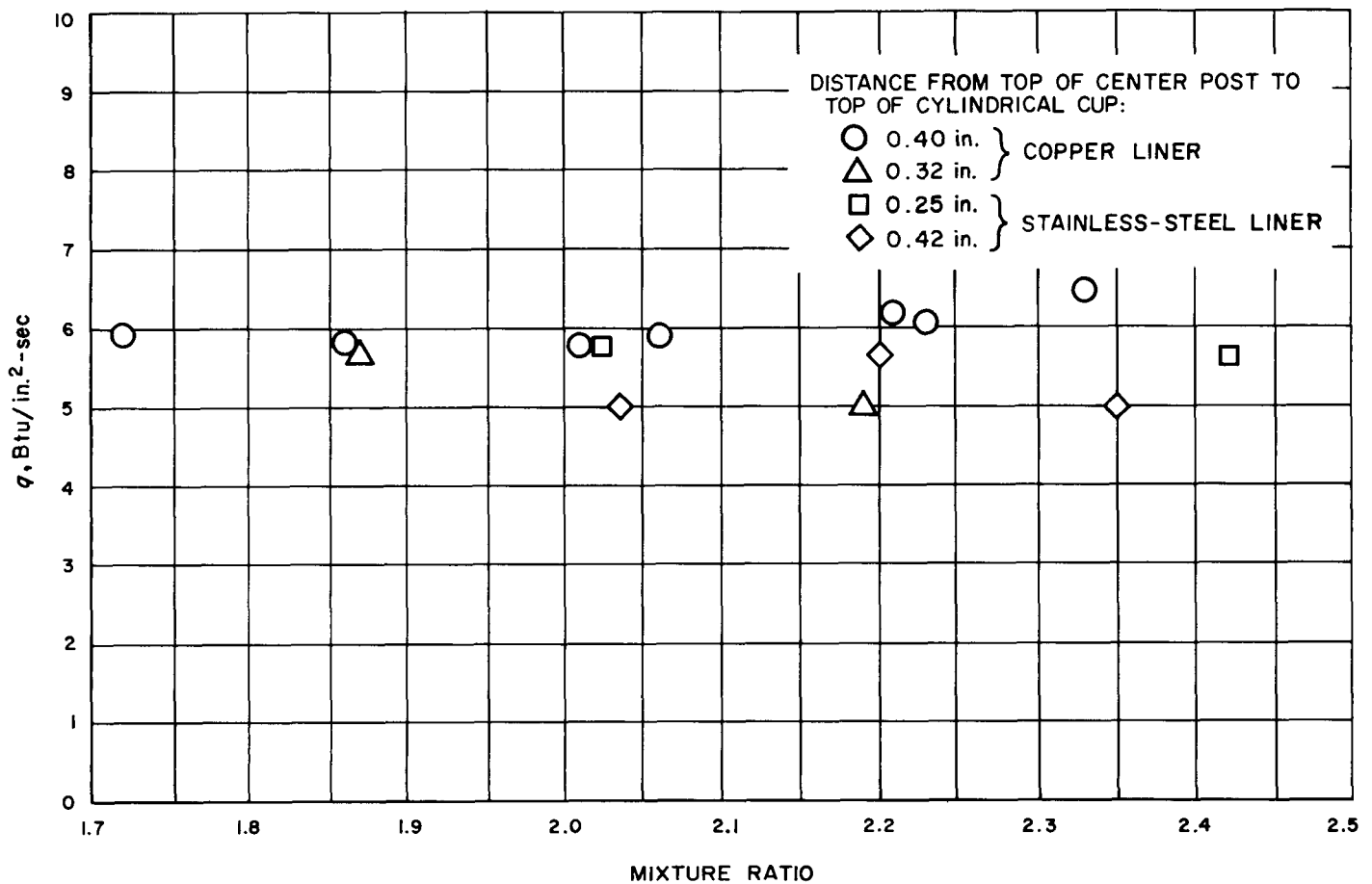
Fig. 24. Average heat flux to section 18 of combustion chamber, 6 to 7 in. from injector face, using
CIF_3-N_2H_4 propellant at approximately 300 psia chamber pressure

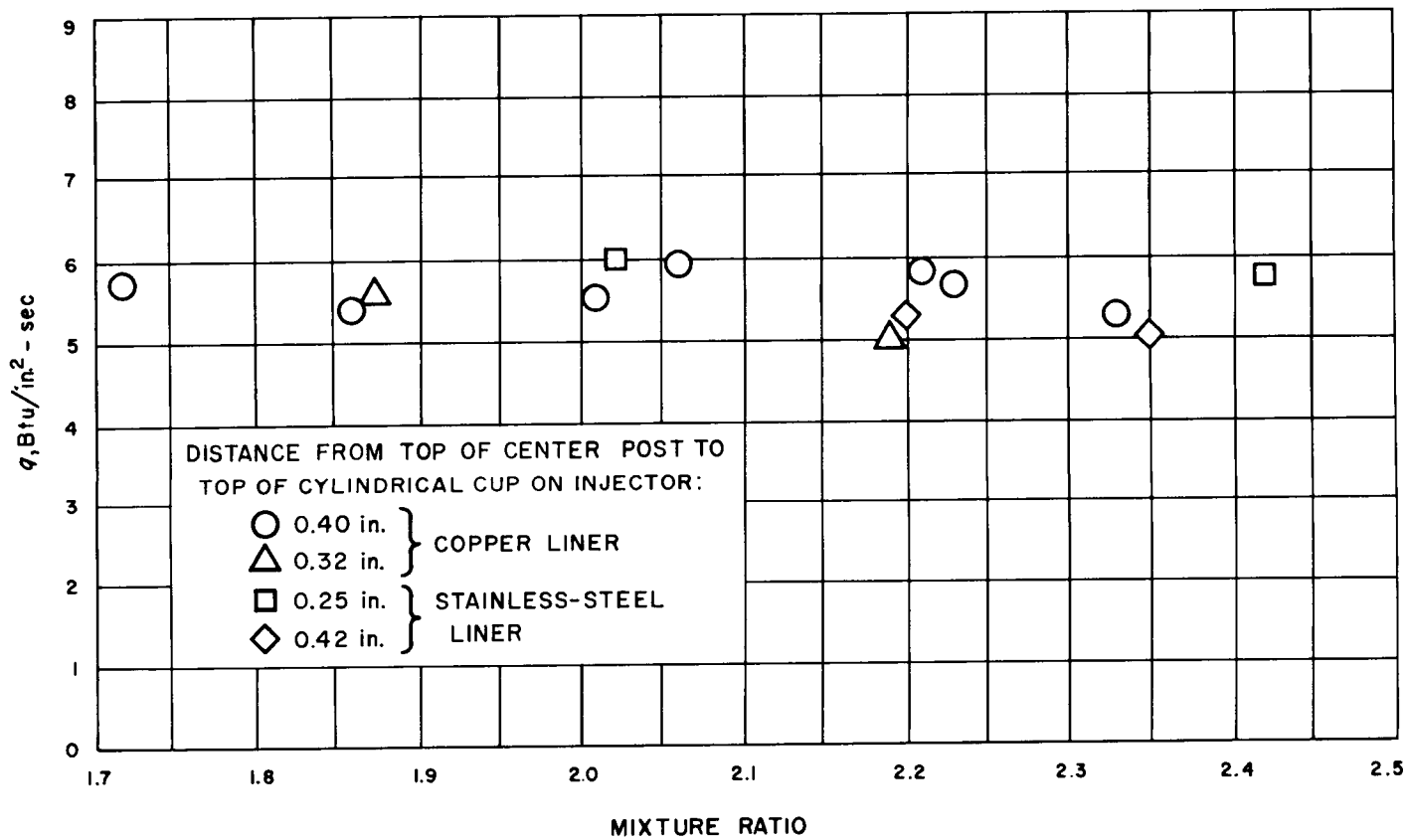Fig. 25. Average heat flux to section 17 of sectional water-cooled combustion chamber, 7 to 8 in. from injector face, using ClF_3-N_2H_4 propellant at approximately 300 psia chamber pressure
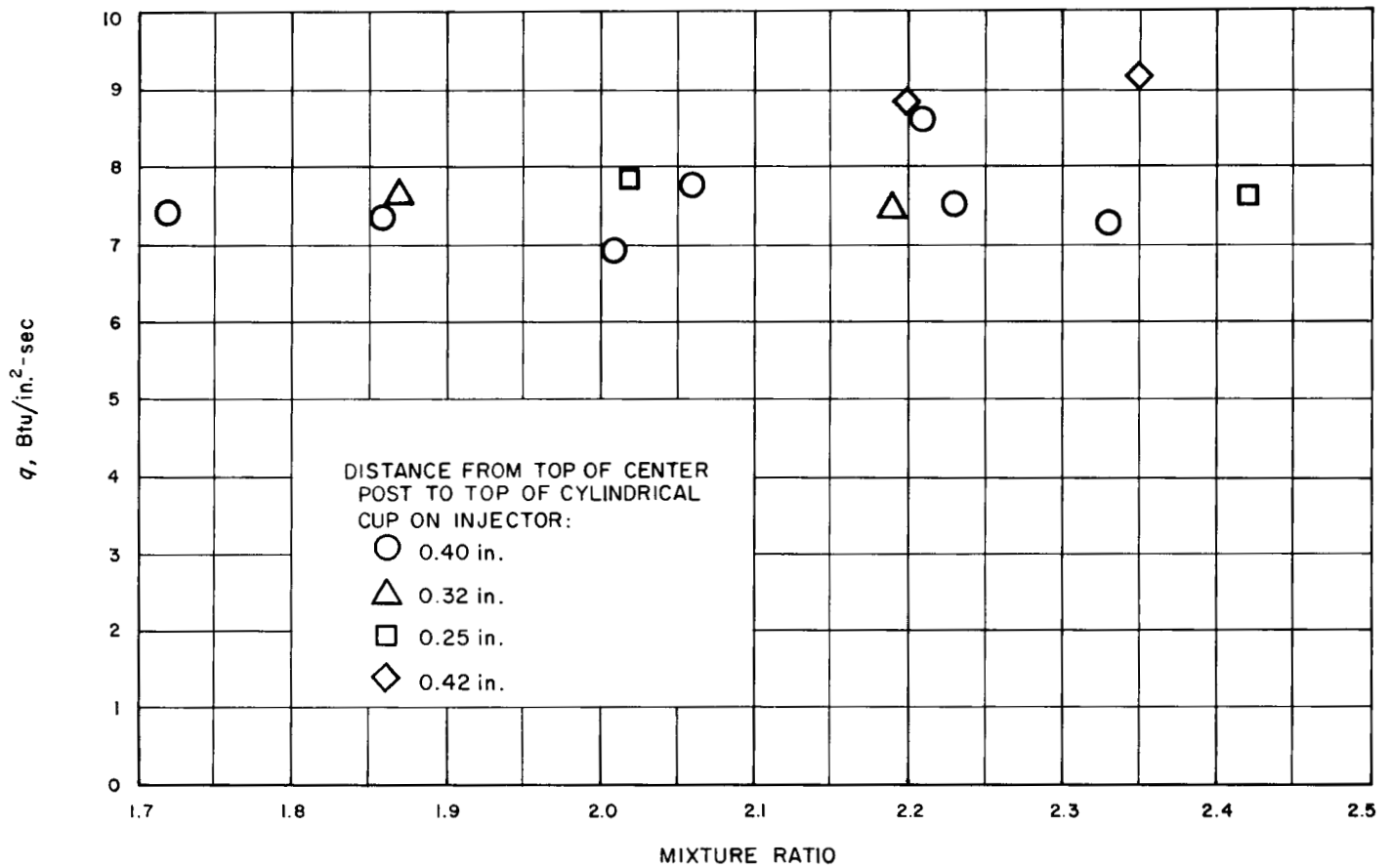
Fig. 26. Average heat flux to section 11, nozzle throat, of sectional water-cooled thrust chamber assembly
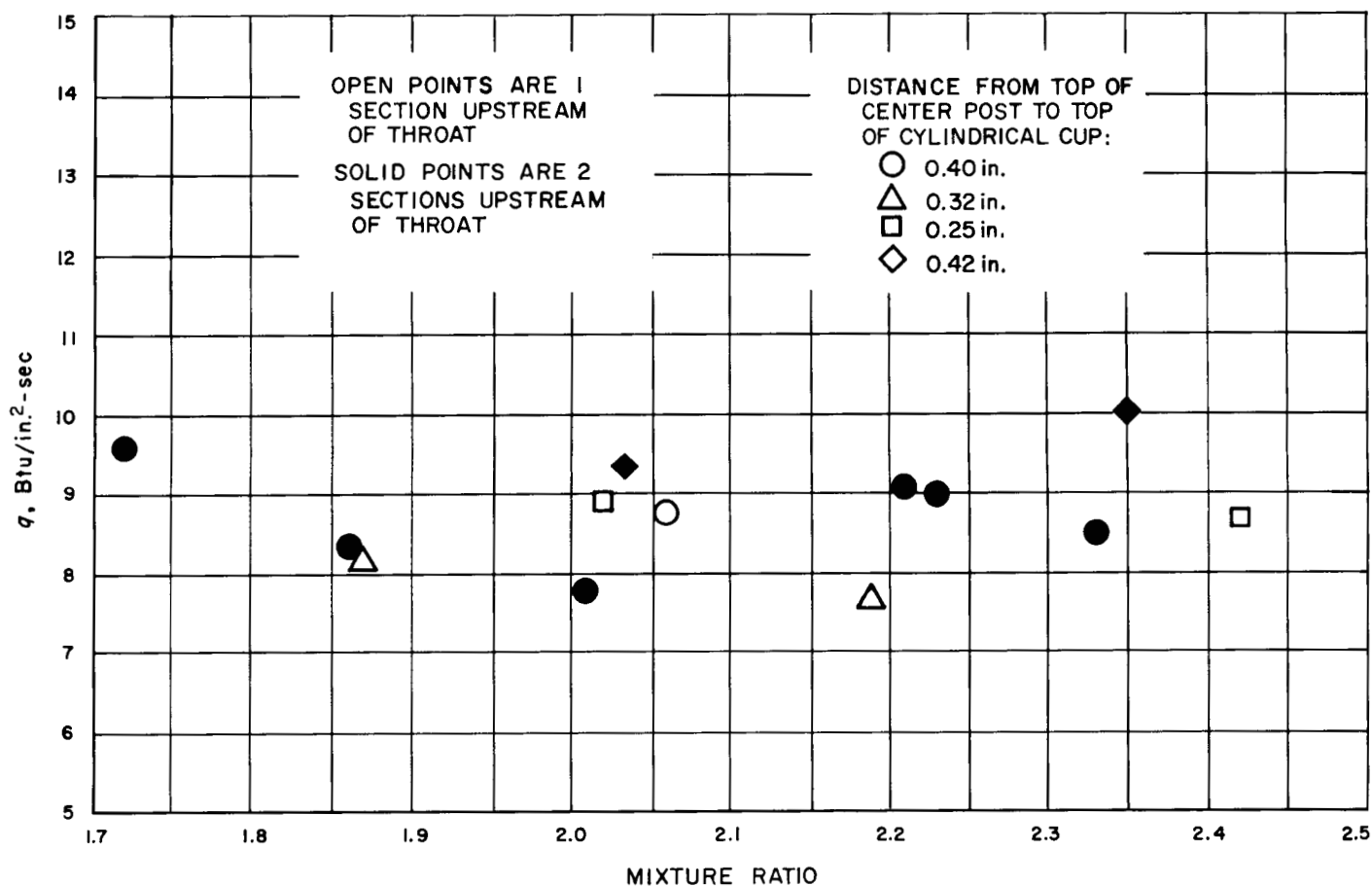
Fig. 27. Maximum average heat flux in nozzle of sectional water-cooled thrust chamber assembly

Table 5. Physical properties of 1020 steel[a][b]

T, °F	c_p, Btu/lb-°F	k, Btu/in.-sec°F
0	0.110	6.95×10^{-4}
100	0.113	6.92×10^{-4}
200	0.117	6.85×10^{-4}
300	0.122	6.72×10^{-4}
400	0.126	6.54×10^{-4}
500	0.131	6.32×10^{-4}
600	0.137	6.08×10^{-4}
700	0.142	5.83×10^{-4}
800	0.150	5.59×10^{-4}
900	0.160	5.35×10^{-4}
1000	0.170	5.08×10^{-4}
1100	0.182	4.79×10^{-4}
1200	0.196	4.50×10^{-4}
1220	0.200	4.45×10^{-4}
1240	0.203	4.40×10^{-4}
1260	0.210	4.34×10^{-4}
1280	0.221	4.28×10^{-4}
1300	0.237	4.22×10^{-4}
1310	0.250	4.19×10^{-4}
1320	0.265	4.16×10^{-4}

a "The Physical Properties of a Series of Steels—Part II", The Iron and Steel Institute, London, 1947.
b $\rho = 0.284$ lbm/in³

wall. Figure 9 shows the installation of a plug which contains a thermocouple located 0.020 in. from the inside surface of the chamber. The plug was made of the same material as the chamber wall, so that the thermal properties of the plug and adjacent wall materials were the same. The inner thermocouple junction was made by flash welding 0.005-in. D insulated chromel and alumel wires, respectively, into the bottoms of holes which were drilled from the sides of the plug toward its axis in such a manner as to leave only a thin web of material at the center. The wires were laid and cemented in small slots along the side of the plug and came out at the outside end of the plug, where they were connected to a terminal block. The ¼-in. D plug was pressed into a tightly fitting hole in the chamber to such a depth that the thermocouple junction was 0.020 in. from the inner surface, and then the projecting tip of the plug was finished off flush with the adjacent chamber surface. The exact final location of the inner thermocouple in such an installation is not accurately known, partly due to limitations in accuracy in measuring the location of the junction and in installing the plug, and partly because of erosion of the chamber wall during repeated testing. The first six tests of the uncooled motor reported herein were made with a thermocouple plug of the above described type inserted in the combustion chamber wall.

In all subsequent tests with the uncooled motor a surface thermocouple was used; the simplification of the data-reduction computing procedure and the elimination of errors associated with the extrapolation of the temperature profile made the development of the surface thermocouple experimental technique desirable. The surface thermocouple is formed by inserting through the chamber wall a plug which contains two separate insulated thermocouple wires parallel to its axis. The plug is trimmed off flush with the inside surface of the chamber and the junction between the two thermocouple wires is made by depositing a thin plating of metal over the plug and the surrounding chamber surface. The surface plugs used in this test series were improvised from commercial thermocouple plugs[8] in which the insulated wires were sealed in the mild steel plug by swaging the steel down around them. For the first attempt, an electroplated copper film was applied to the inside surface of the chamber to bridge the ends of the thermocouple wires. Later, an electroless nickel-plating process, described in Ref. 6, was used to deposit a film of nickel approximately one ten-thousandth of an inch thick in the area of the thermocouple. Fifteen tests were made with surface thermocouple inner wall temperature measurements on the uncooled motor combustion chamber.

The six tests with the recessed thermocouple plugs and the first three tests with the surface thermocouples were made without noting the circumferential location of the thermocouple with respect to the peripheral elements of the injector. The twelve subsequent tests with the surface thermocouple were made with the thermocouple either directly in line with or directly between adjacent injector elements.

Typical heat-flux data obtained from uncooled combustion chambers, using the thermocouple plug technique are shown in Fig. 28, 29 and 30. There is a starting transient time of almost half a second, during which steady-state propellant flow rates and combustion chamber pressure and temperature are being established. During this time, the heat flux and the wall temperature are both increasing. When steady-state combustion and the corresponding chamber gas stagnation temperature and heat-transfer coefficient are established, the heat transfer starts to decrease, corresponding to the decrease in driving potential as the wall temperature continues to rise. In Fig. 28, 29 and 30, a wall temperature of 700 to 900°F is attained during the starting transient; above these tem-

[8]Advanced Technology Laboratories, Mountain View, Calif.

in the nozzle has no significant trend with mixture ratio, but the scatter of the data is broader than that in the chamber; maximum measured nozzle heat flux ranges from 7.7 to 10.0 Btu/in.²-sec. In 7 of the 9 tests with the longer cups (0.40- and 0.42-in. cup extension) the peak flux occurred two sections upstream of the throat, while on all other tests the peak occurred one section upstream of the throat. This may indicate better combustion with the long cups.

The low thermal conductivity of stainless steel results in an appreciable increase in gas-side wall temperature of a stainless-steel-lined water-cooled chamber section, compared to that of a section having a copper liner. In the motor tested the chamber inner-wall temperature was approximately 370°F for a copper-lined section with a heat flux of 5.8 Btu/in.²-sec and 1100°F for a stainless-steel-lined section with a heat flux of 5.4 Btu/in.²-sec. An approximate calculation, taking into account the difference in the temperature potential for heat transfer and the effect of a decrease in gas-side heat-transfer coefficient with an increase in temperature of the boundary layer, indicated that the stainless-steel-lined section, with its higher wall temperature, might have a heat flux about 20% less than that of the corresponding copper-lined section. The difference in the experimental heat flux corresponding to the two liner materials is distinguishable on Fig. 24 and 25, but is considerably less than the predicted difference, which was based on a number of simplifying assumptions.

B. Chamber Heat Flux From Transient-Temperature Measurements in Uncooled Motor Wall

The determination of local heat flux to the wall of a combustion chamber from data obtained while the wall is being heated during a short duration motor test is based on the solution of the equation for transient heat conduction in a one-dimensional axisymmetric hollow cylinder having variable, but known, thermal properties. If the temperature-time histories of two points on a radial path in the cylinder are used as boundary conditions, solutions of this equation gives the complete temperature distribution of the region between the two points as a function of time. For determining heat transfer from combustion gases to the inside wall of a combustion chamber, one of the measured temperatures should be at or near the inner surface of the chamber. Then an analytic function can be fitted to the temperature distribution between the points at which temperature is measured, and the temperature at the wall can be found,

if necessary, by a short extrapolation of this function. The temperature gradient at the wall is then found by differentiating the analytical function, and the heat flux at the wall is computed using the gradient and the thermal conductivity at the wall.

The basic equations are

$$\rho\, c_p \frac{\partial T}{\partial t} = \frac{\partial}{\partial r}\left(k\, \frac{\partial T}{\partial r}\right) + \frac{k}{r}\, \frac{\partial T}{\partial r} \tag{1}$$

and

$$q_w = -\, k_w \left(\frac{dT}{dr}\right)_w \tag{2}$$

The transformation of Eq. (1) into a difference equation and the technique of numerical solution using a digital computer are described in Ref. 5. This reference contains a discussion of the accuracy of the computed surface heat flux as influenced by variations in the details of the method of calculation and by the various experimental errors which may be incorporated in the information supplied to the digital computer.

The outputs of the thermocouples measuring the wall temperatures were amplified, digitalized, and recorded on magnetic tape, using a Consolidated Systems Corp. MicroSADIC digital data recorder. The output of each thermocouple was recorded every 0.013 sec. The digital data recorded on the magnetic tape was used directly as input to the digital computer, an IBM 704. Geometrical configuration and tabular information on the physical properties of the material of the wall as a function of temperature constituted the remainder of the input to the digital computer.

The uncooled chambers used in the ClF₃-N₂H₄ tests were made of mild steel pipe having a composition and physical properties closely approximating those of SAE 1020 carbon steel. The thermal properties of this steel, as used in the calculation procedures, are given in Table 5. The chamber sections had 5-in. ID and a wall thickness of ⅝ in. The 2-in.-long chamber instrumentation section, in which the wall temperature thermocouples were inserted, is shown in the uncooled motor assembly drawing (Fig. 9). In the 8-in. chamber length motor, the thermocouples were installed 7 in. from the face of the injector.

One thermocouple was spot-welded to the outside surface of the chamber. The other wall temperature measurement was made on, or near, the inside surface of the chamber by means of a thermocouple which was built into a small plug which was inserted into the chamber

peratures the fully developed heat-transfer process exists. If it is desired to find the equivalent heat flux at a lower wall temperature, such as might exist in a cooled combustion chamber, the fully developed heat transfer portion of the data must be extrapolated. Thus, in Fig. 28, heat transfer is fully developed 0.52 sec after the motor is started; the wall temperature is 850°F and the heat flux is 6.55 Btu/in.²-sec. At 1100°F the heat flux is 5.75 Btu/in.²-sec, and extrapolating back to 400°F wall temperature, a cooled combustion chamber having this wall temperature would appear to have to be designed to absorb a heat flux of 8.4 Btu/in.²-sec.
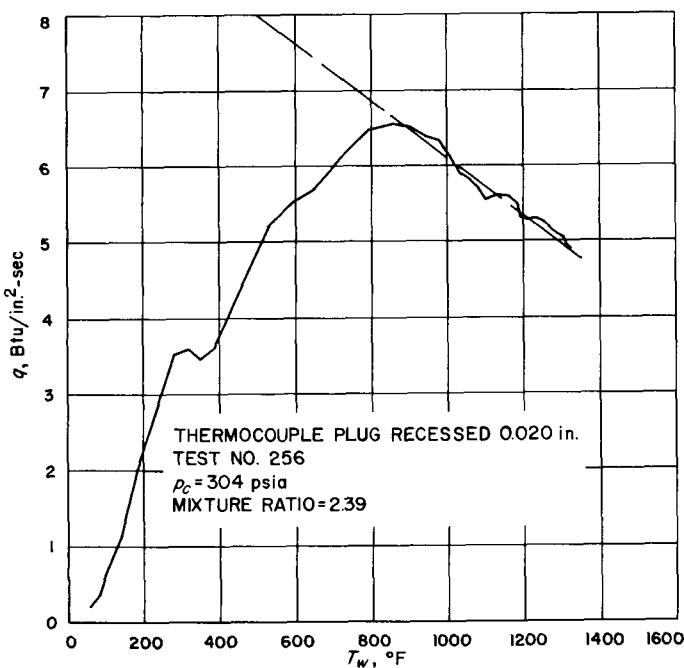

Fig. 28. Local heat flux to combustion chamber of ClF₃-N₂H₄ rocket motor

The heat flux obtained from the thermocouple-plug-instrumented tests of the uncooled motors is shown for wall temperatures of 1100 and 400°F in Fig. 31 and 32. The heat flux at 1100°F is obtained directly from the plots of the experimental data. The heat flux at 400°F is obtained by extrapolating the fully developed heat-transfer portion of the experimental data back to the 400°F wall temperature, as described previously and illustrated in Fig. 28, 29, and 30.

Figures 31 and 32 show data which were obtained using both recessed and surface thermocouple plugs having unknown orientation with respect to the injector elements, data obtained using surface thermocouple plugs which were directly downstream of the injector
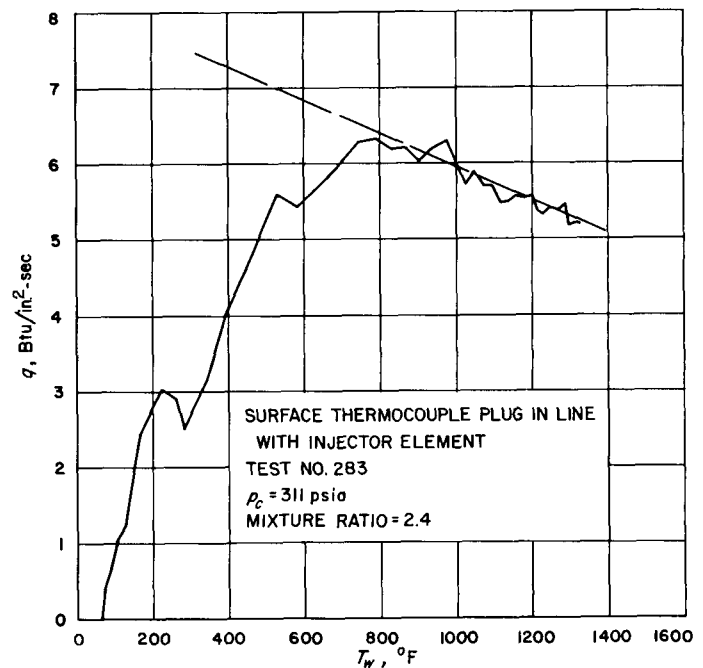

Fig. 29. Local heat flux to combustion chamber of ClF₃-N₂H₄ rocket motor

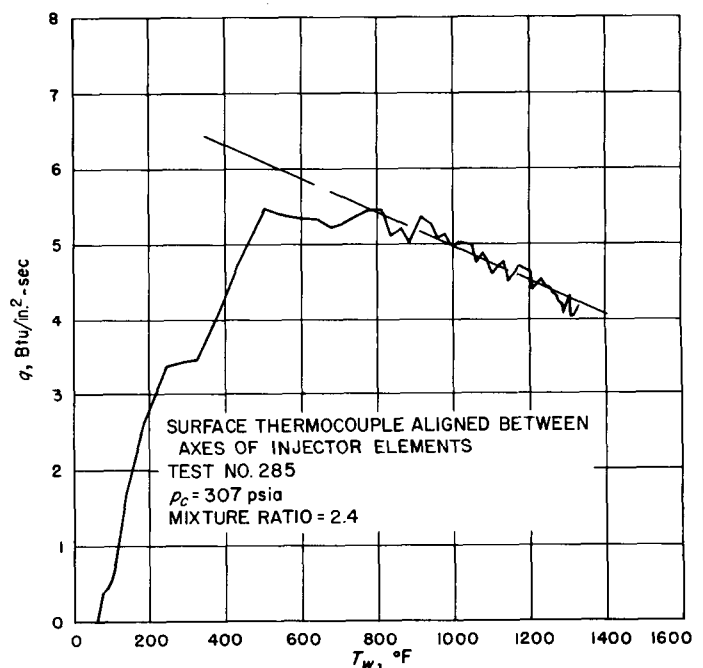**Fig. 30. Local heat flux to combustion chamber of ClF₃-N₂H₄ rocket motor**

elements, and data obtained using surface thermocouple plugs which were located downstream of a position in-between injector elements. In Fig. 31 it can be seen that the heat flux obtained with the surface thermocouple
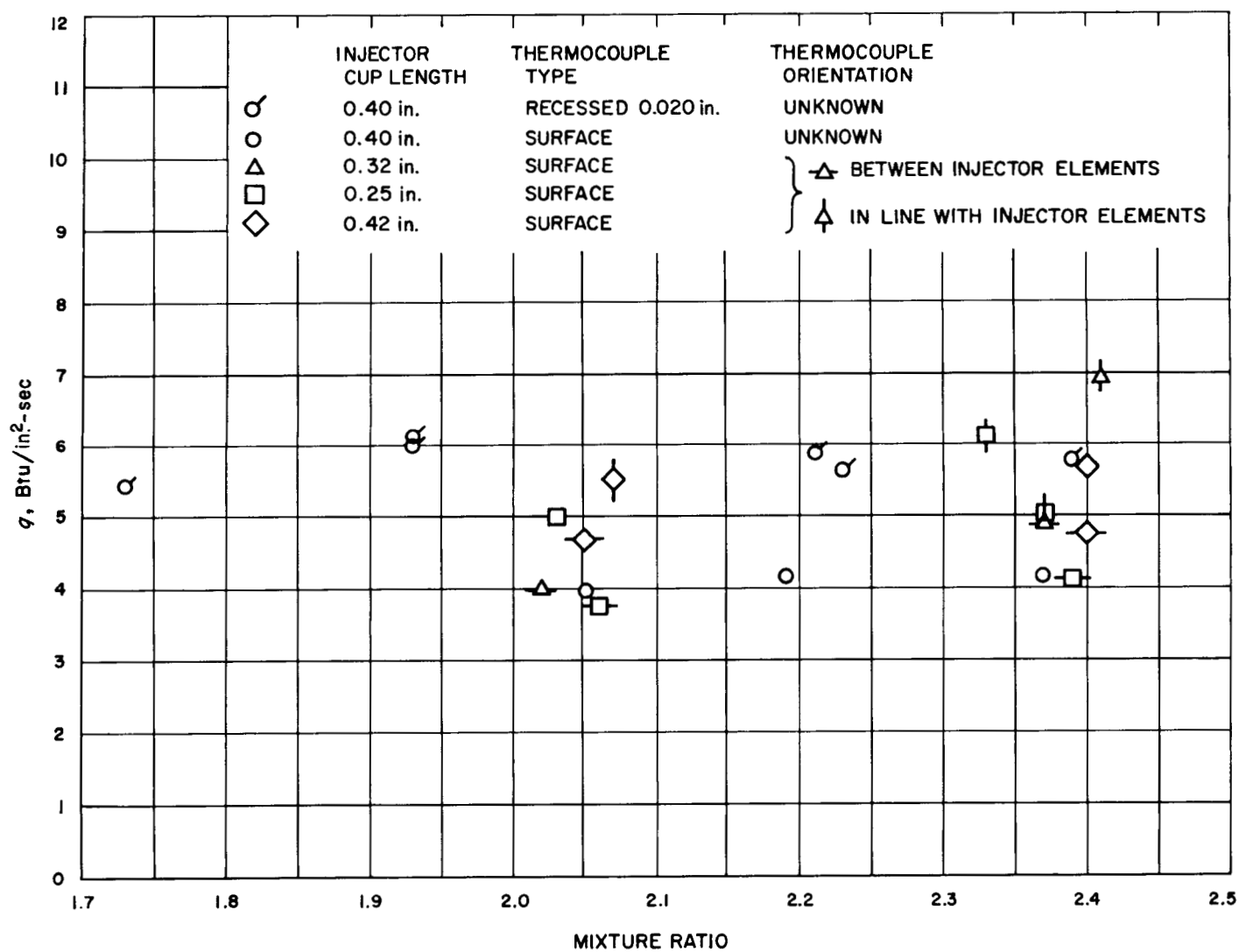
Fig. 31. Local heat flux in uncooled combustion chamber 7 in. from face of injector,
determined by thermocouple plug technique. Wall temperature, 1100° F.
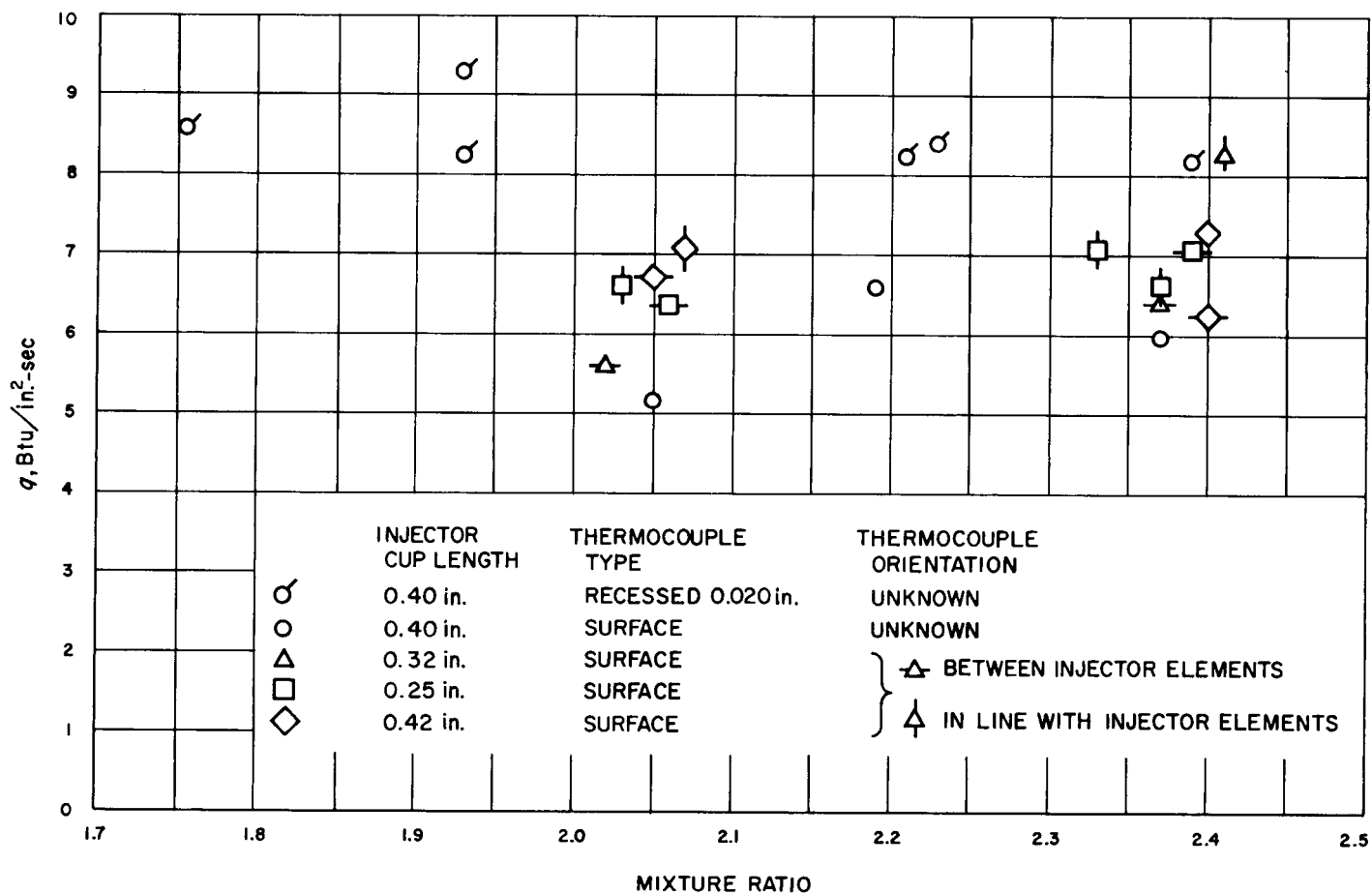
Fig. 32. Local heat flux in uncooled combustion chamber 7 in. from face of injector, as determined by extrapolating results of thermocouple plug calculations. Wall temperature, 400° F.

plugs in line with the injector elements is consistently higher than that obtained when the thermocouple plugs were located in-between the injector elements. Since the design of the injector is such that local variations in chamber heat flux might be expected, it is believed that this technique accurately reflects the relative local flux. The fact that the separation of the two classes of data is not as complete on Fig. 32 can be ascribed to errors associated with the extrapolation involved. The thermocouple plug average heat flux in the chamber 7 in. downstream of the injector can be estimated from Fig. 31 and 32 as 5.0 Btu/in.²-sec at a wall temperature of 1100°F and as 6.8 Btu/in.²-sec at a wall temperature of 400°F.

At the calculated 1100°F wall temperature of the stainless-steel-lined cooled section, the calorimetric average heat flux is 5.4 Btu/in.²-sec and the thermocouple plug average heat flux is 5.0 Btu/in.²-sec; the thermocouple plug value is approximately 7½ % less than the calorimetric heat flux. This is the type of variation from the true value which would be anticipated from the digital calculation procedure used in reducing the surface thermocouple plug data (Ref. 5). The 7½ % difference between the two measurements is reasonable, especially considering the fact that the thermocouple plug average heat flux was obtained by averaging the data from only two thermocouple plug positions.

At the calculated 400°F wall temperature of the copper-lined cooled section, the agreement between the calorimetric average heat flux of 5.8 Btu/in.²-sec and the average extrapolated thermocouple plug heat flux of 6.8 Btu/in.²-sec is not as good as might be desired, but can be accepted in view of the extrapolation involved. Since the actual heat-transfer process in the combustion chamber may involve liquid droplets as well as hot gases, the extrapolation may not conform to the actual change of heat flux with wall temperature. It would be desirable, in applications of the thermocouple plug technique, to operate the uncooled motor so as to achieve combustion equilibrium before the wall temperature of interest has been exceeded. Then extrapolation can be avoided.

The surface thermocouple technique appears to provide a reliable and fairly sensitive method for the determination of local transient heat flux in an uncooled motor. Further experimental data supporting this conclusion are presented in Ref. 5. Further developments in the technique of collecting and reducing the data may be expected to result in closer agreement between the thermocouple-plug-data-derived heat flux and the calorimetric average heat flux. Results obtained with the surface thermocouple are believed to be better than those obtained with the recessed thermocouple, where the position of the recessed thermocouple junction is usually not accurately known and the data analysis calculation procedure involves an extrapolation which may introduce errors. The surface thermocouple is not without its faults, however. Erosion of the thin layer of nickel plate, which formed the contact between the thermocouple wires, necessitated replacement or replating after four to six tests.

IX. CONCLUSIONS

Chlorine trifluoride–hydrazine rocket motors have been operated successfully and the potential usefulness of this propellant has been substantiated.

Chlorine trifluoride has been handled without incident involving personnel during a test program lasting over three years. Handling techniques and cleaning procedures which make feasible the use of this potentially hazardous chemical as a rocket propellant have been developed and applied.

A rocket motor has been operated with the chlorine trifluoride–hydrazine propellant and an effective exhaust velocity of 7580 ±80 ft/sec has been demonstrated over a wide mixture ratio range ($r = w_o/w_f = 1.7$ to 2.4), using either an uncooled (short duration test) motor or a water-cooled motor. The injector developed during the program and used for these tests was cooled by the incoming propellants. Both the exposed elements of the injector and the water-cooled copper exhaust nozzle were gradually attacked or eroded by the hot combustion gases, and had an approximate useful lifetime of 70 to 100 sec. Heat transfer rates of 5 to 6 Btu/in.²-sec in the chamber, with a maximum flux of 8 to 10 Btu/in.²-sec just upstream of the nozzle throat are high but not excessive.

Despite the advantages of chlorine trifluoride–hydrazine as a high-density storable propellant giving moderately high performance, two serious problems are associated with its potential use:

1. The propellant and its combustion products are highly corrosive. While water-cooled chamber sections, lined with copper or stainless steel, operated satisfactorily, the aluminum cups of the injector and the copper liners of the exhaust nozzle were attacked and had a limited lifetime in operation. Additional development may be required for applications where long duration or repeated operation is required.

2. Chlorine trifluoride is a very poor coolant, having a low specific heat and a heat flux at the upper limit of nucleate boiling of 2.5 to 6.0 Btu/in.²-sec over a range of temperature, pressure, and velocity (Ref. 1). At the same time the proportion of hydrazine available in the operating mixture ratio range is such that its total heat absorbing capacity is insufficient to regeneratively cool a motor of the 5000-lb thrust scale such as was used in the present tests. It is estimated that thrust level would have to be increased somewhat more than an order of magnitude, to 80,000- or 100,000-lb thrust, before straight regenerative cooling of a chlorine trifluoride–hydrazine rocket motor becomes feasible.

The chlorine trifluoride–hydrazine rocket propellant has a high average density, is storable, and gives good performance. On the other hand, the oxidizer is an extremely active chemical, so that parts exposed to it must be thoroughly cleaned and special handling precautions must be used; the combustion products are erosive, and the regenerative cooling capacity of the propellant is limited. The outstanding advantage of this propellant over other propellants is in its higher average density; its application should generally be limited to situations where high density is a major requirement and where long-duration operation and regenerative cooling are not required. This suggests the use of this propellant combination with uncooled or ablative motors of low and medium thrust levels in one-shot applications.

NOMENCLATURE

A_c cross-sectional area of cylindrical combustion chamber

A_e cross-sectional area at exit of nozzle

A_t cross-sectional area at throat of nozzle

c_{eff} effective exhaust velocity

c^* characteristic velocity

C_F thrust coefficient

c_p specific heat

C' venturi flowmeter calibration coefficient

d_1 diameter of line upstream of flowmeter

F thrust

g acceleration due to gravity

k thermal conductivity

p_c effective chamber pressure; isentropic stagnation pressure at throat of nozzle

p_t pressure at throat of venturi flowmeter

p_{up} pressure upstream of flowmeter

p_2 chamber pressure at downstream end of cylindrical combustion chamber

q heat flux

r propellant mixture ratio, wt. oxidizer/wt. fuel

r radius

Re Reynolds number

t time

T temperature

w weight flow rate

γ specific weight

ρ mass density

μ viscosity

Subscripts

f fuel

o oxidizer

th computed value, ideal

w value at inside surface of combustion chamber

APPENDIX A

Injector Configurations Tested

Several injectors were fabricated and tested before the multi-element cup and plug design with which the test series was concluded was evolved. This Appendix contains a brief description of these injectors and of the results obtained with them.

I. TWO-ON-TWO IMPINGING STREAM INJECTOR

This injector was used for the first 20 tests to shake down the ClF_3-N_2H_4 installation when it was first put into use. It consisted of a heavy uncooled plate with openings for four symmetrically spaced, replaceable orifices whose axes were inclined at 45 deg. to the centerline of axial symmetry of the injector; the liquid streams intersected approximately 1 in. from the face of the injector plate. It was piped up to supply opposite pairs of orifices with chlorine trifluoride and hydrazine respectively. The impingement of the four large propellant streams at a 90-deg. included angle resulted in the formation of a dense central core-flow of propellant, of large droplets, and of considerable back-splash.

The result was a rough-running motor having low performance and an erosion problem on the injector face plate.

II. NINE-ELEMENT INJECTOR

This injector is shown in Fig. A-1, A-2, and A-3. There are eight triplet impinging stream elements arranged symmetrically around the circumference of the injector. At the center of the injector face is a four-on-one orifice element. All of the orifices are removable and replaceable, so that orifice sizes can be changed or orifices can be blanked off when desired. The orifices extend through the cooled face plate of the injector and are connected to propellant manifolds supported behind the face plate. Water used for cooling the injector face enters and leaves through the radial fittings on the edge of the flange.

This injector was tested in a number of configurations, with and without the central four-on-one element, and with plain and slotted splash plates deflecting the propellant from the outside row of eight triplet elements.

While this injector appeared capable of giving fairly high performance with the ClF_3-N_2H_4 propellant, it was extremely rough in operation. Further difficulties were the repeated erosion of the injector face and of the walls of the uncooled mild steel combustion-chamber sections which were used. In addition, it was difficult to prevent and to repair leaks which developed in the tubing between the injector orifices and the propellant manifolds.
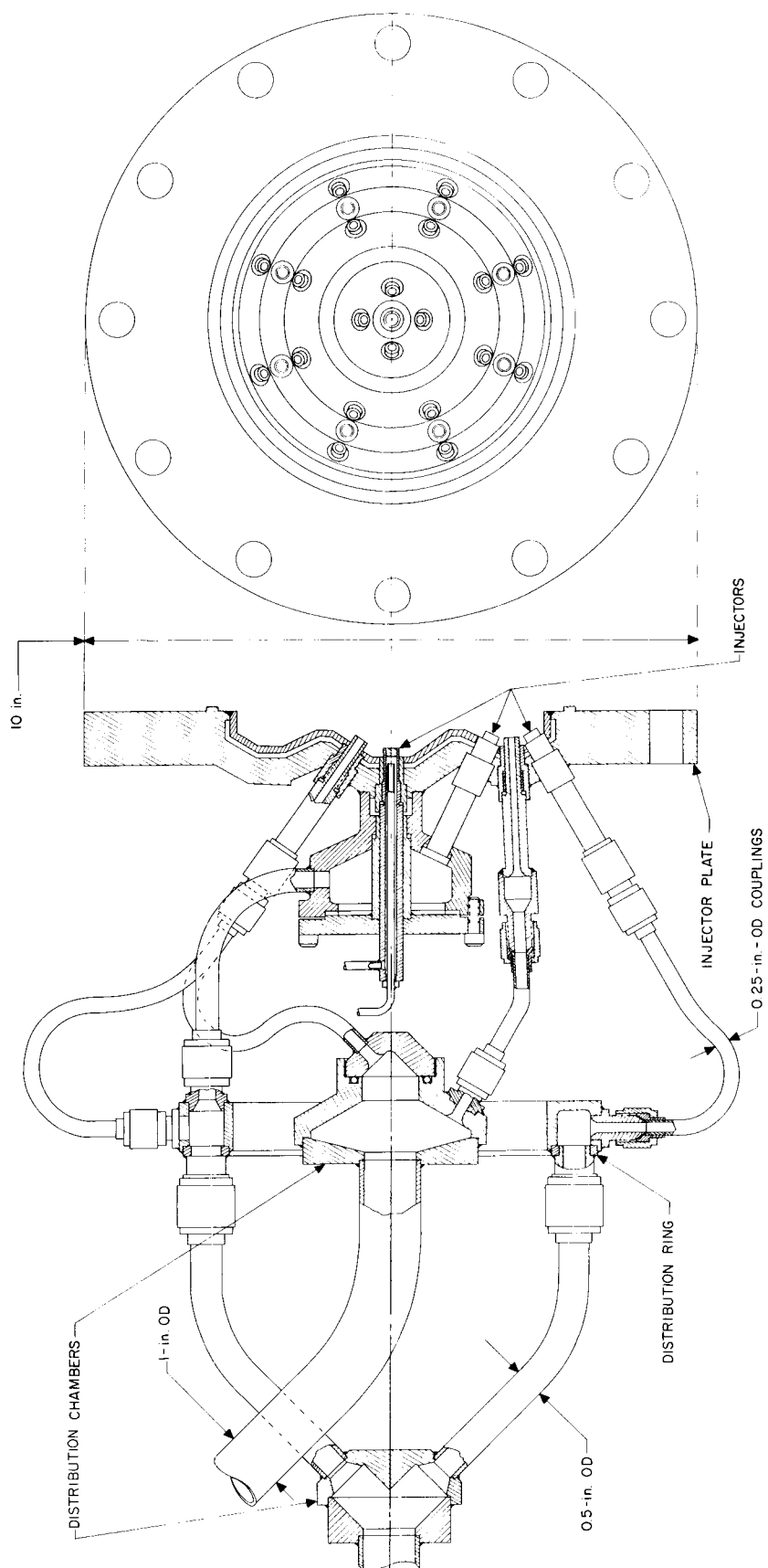
Fig. A-1. Injector with eight triplet elements and four-on-one element in center, section showing propellant manifolding
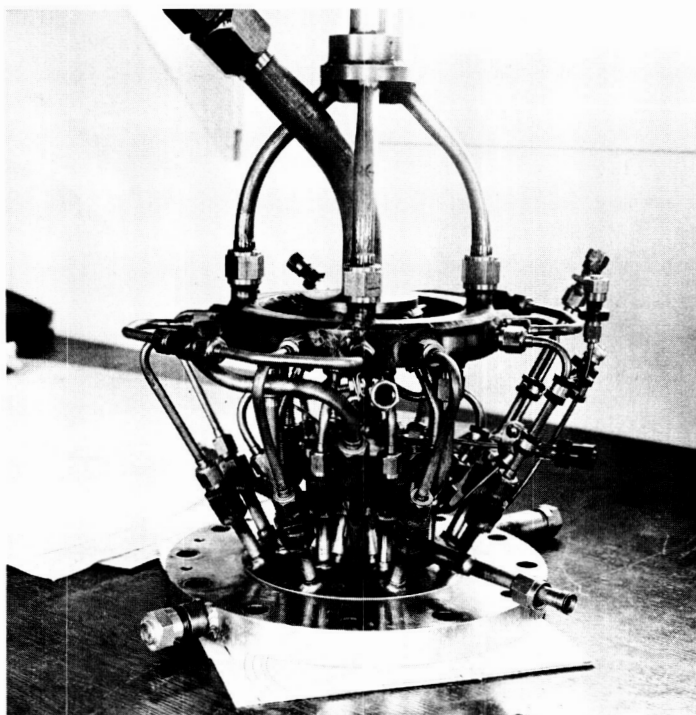
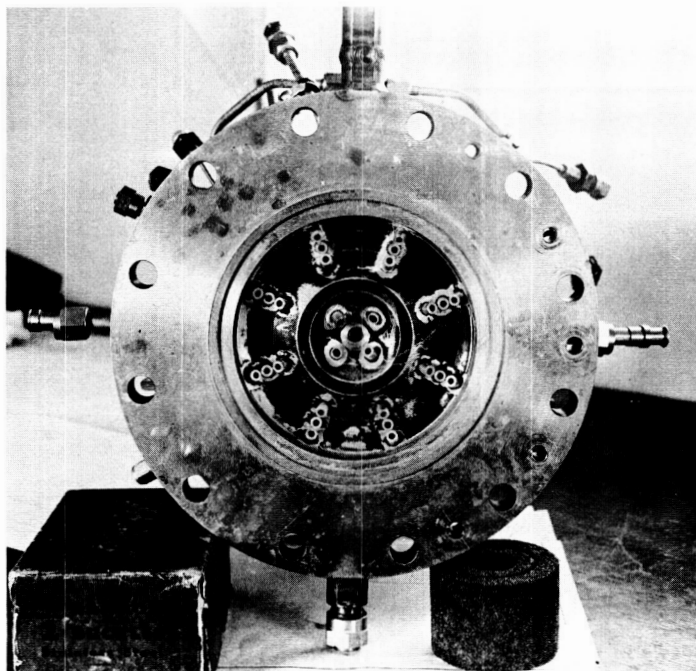Fig. A-2. Propellant manifolding of nine-
element injector

Fig. A-3. Injector with eight triplet elements and four-
on-one element in center, face view

III. ANNULAR IMPINGING SHEET-SPRAY INJECTOR

The annular impinging sheet-spray injector was designed to utilize thin-sheet impingement for mixing in a constricted region where gas velocities were high and recirculating gas flows were inhibited. Good performance was obtained from this injector when the oxidizer was injected through the outer row of orifices, but there was erosion of the central cone. Several modifications of this injector were tested, involving changes in the angle of the deflection surfaces and in the size of the central cone. Erosion remained a problem, and roughness developed in some mixture ratio ranges. Fig. A-4 shows the design of this injector and Fig. A-5 shows erosion of the central plug and of the divider between the orifices after several tests.
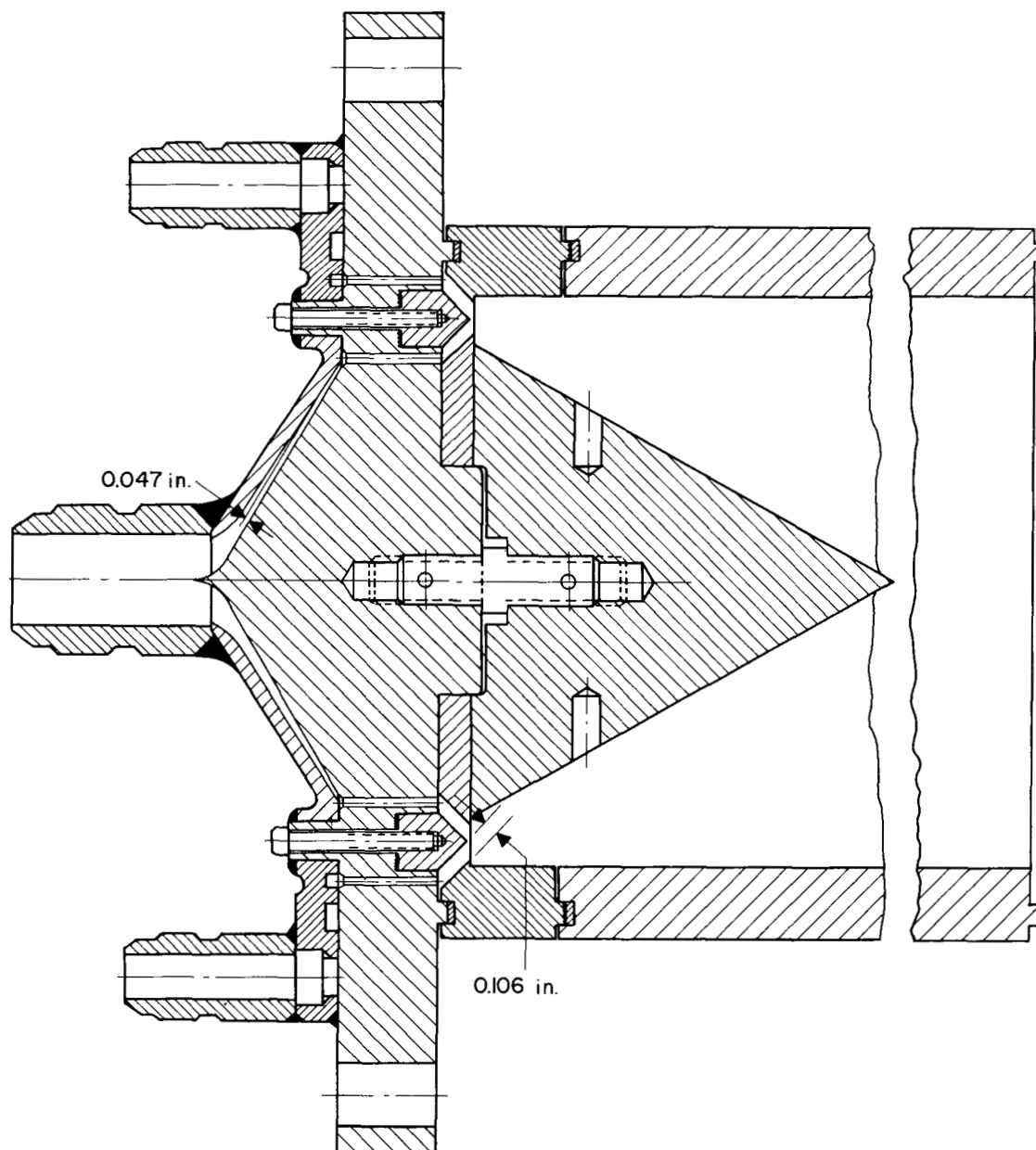

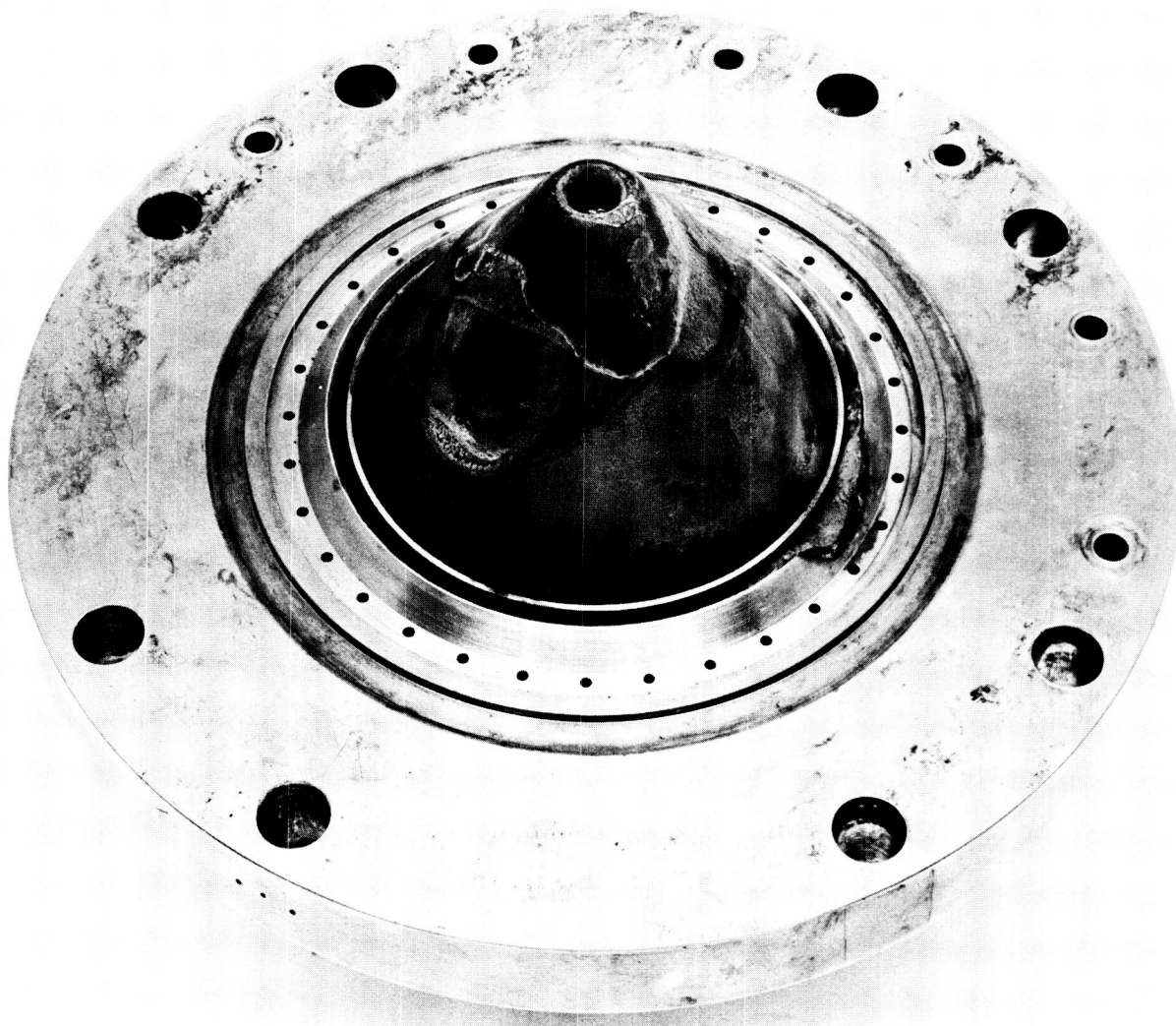**Fig. A-4. Assembly drawing of annular impinging sheet-spray injector and combustion chamber**

Fig. A-5. Erosion of annular impinging sheet-spray injector after several tests

IV. CONCENTRIC ANNULUS PRE-MIX INJECTOR

The concentric annulus pre-mix injector is shown in Fig. A-6. The two propellant component annular sheets were mixed together and then the mixture was deflected outward toward the wall of the combustion chamber. The initial tests with this injector yielded low performance. Several modifications of this injector, including
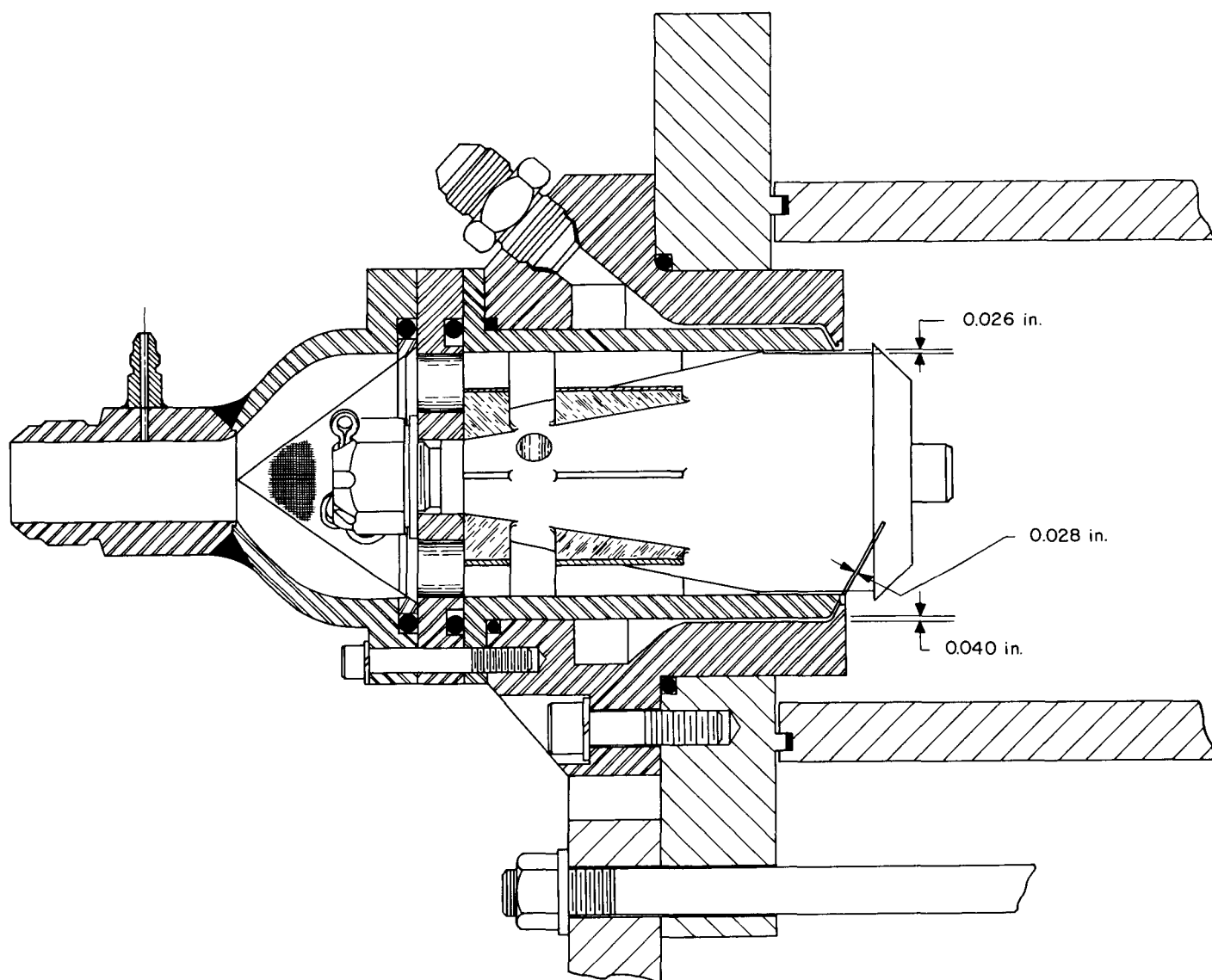
Fig. A-6. Concentric annulus pre-mix injector

changes in the deflector plate and in the manner of mixing of the propellant sheets (Fig. A-7) failed to improve the performance.

It was during a test with this injector that sudden admission of chlorine trifluoride into the central propellant manifold resulted in a minor explosion (Fig. A-8). It was reasoned that the sudden propellant admission had caused an adiabatic compression of the gas within the manifold, producing temperatures sufficient to cause the ClF_3 to react with the stainless steel filter screen in the injector. The injector was rebuilt and was operated successfully using a nitrogen purge which was displaced by the propellant flow, as described in the text of this Report. However, performance remained low and this injector was dropped in favor of later designs.
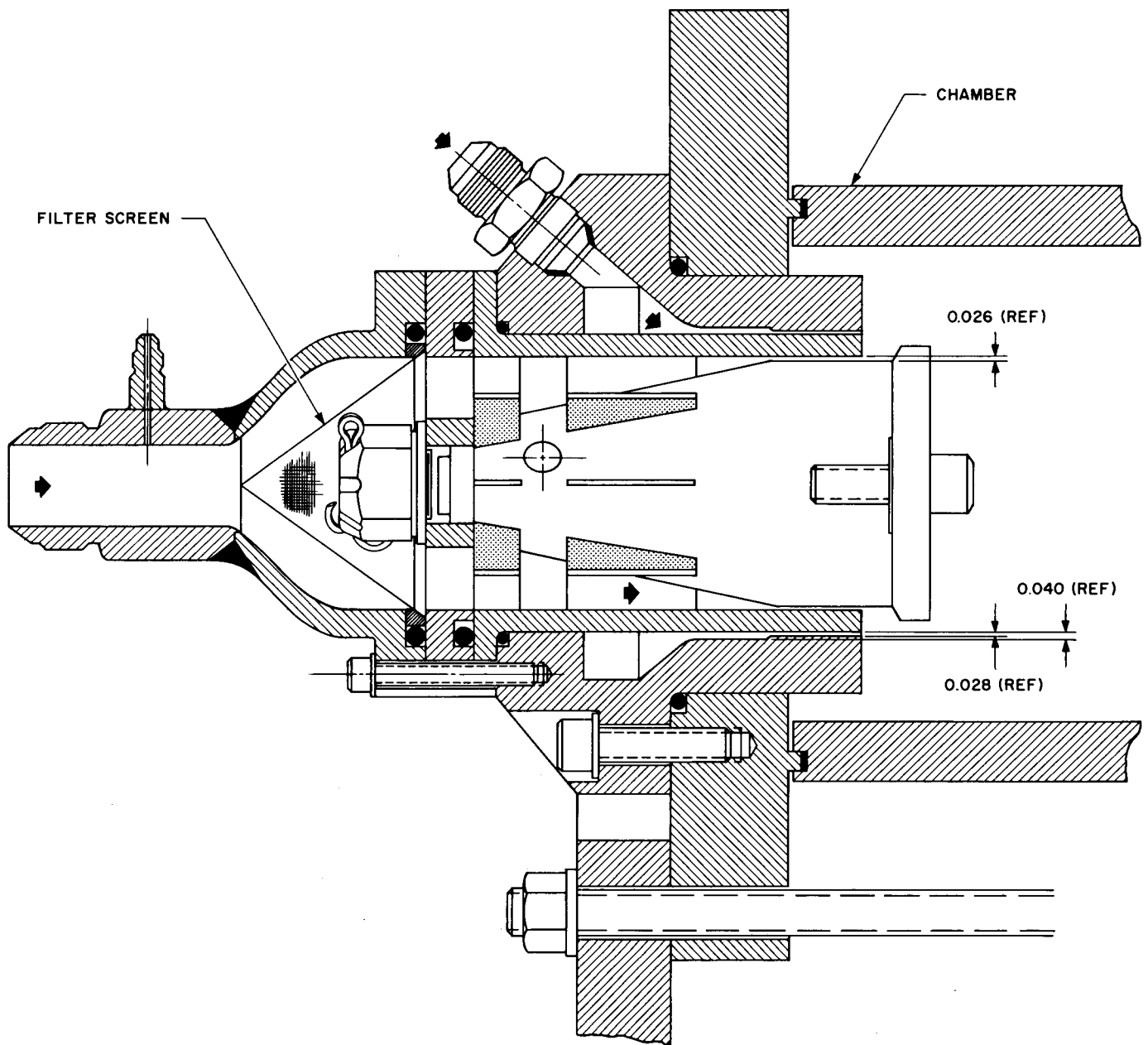
CHAMBER

FILTER SCREEN

0.026 (REF)

0.040 (REF)

0.028 (REF)

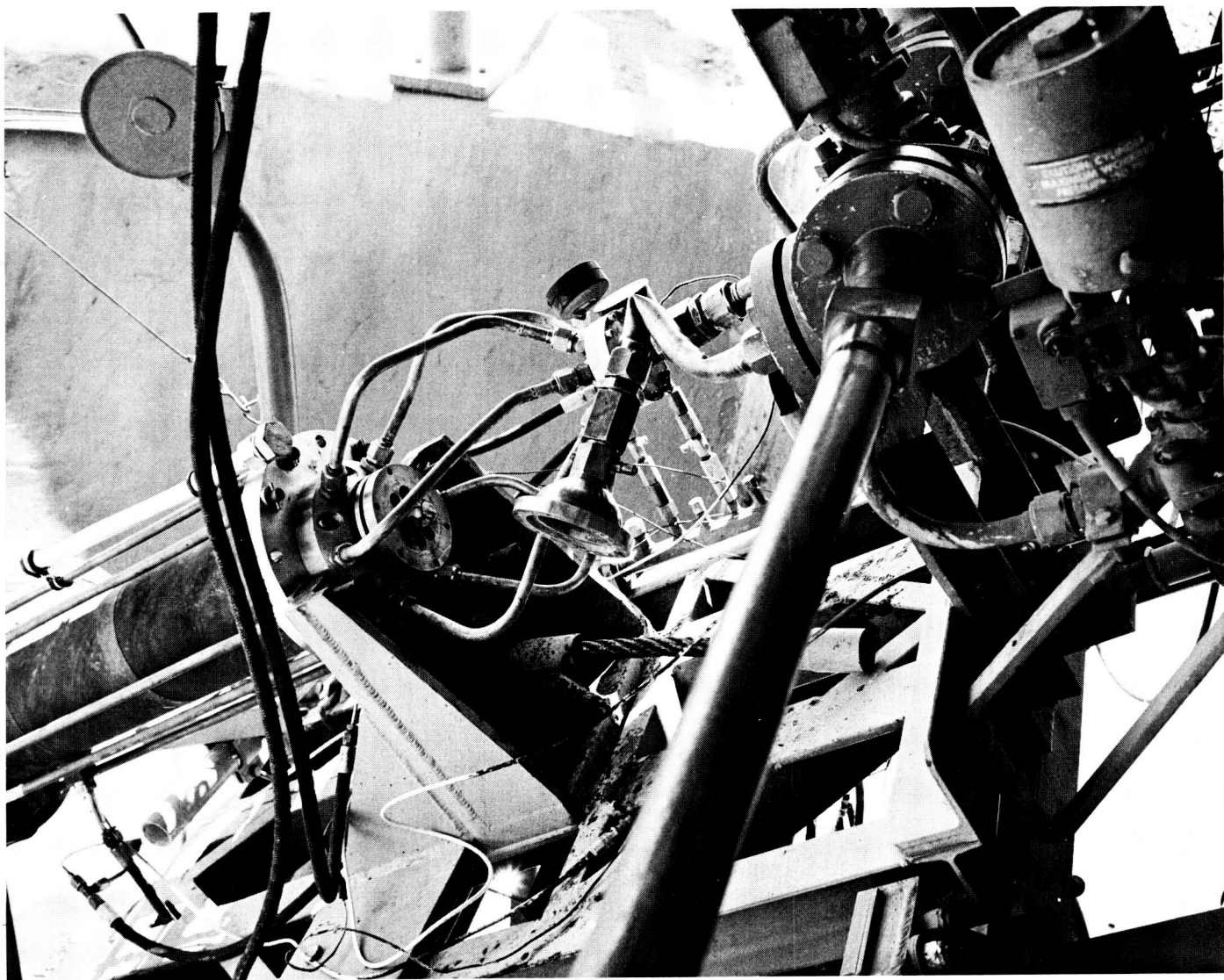Fig. A-7. Modification of concentric annulus pre-mix injector

Fig. A-8. Effect of ClF₃ reaction with screen in inlet manifold of concentric annulus pre-mix injector

V. CONICAL SHELL-MULTITRIPLET INJECTOR

The conical shell-multitriplet injector is shown in Fig. A-9. The conical back face of the injector was inset with triplet element manifold bars, so that propellant was introduced in many small triplet fans normal to the surface of the cone over a large part of the surface of the cone. Each triplet manifold bar was drilled with a line of triplet orifice groups spaced 0.20 in. apart. In this line of triplets, each element was canted 15 deg., so that
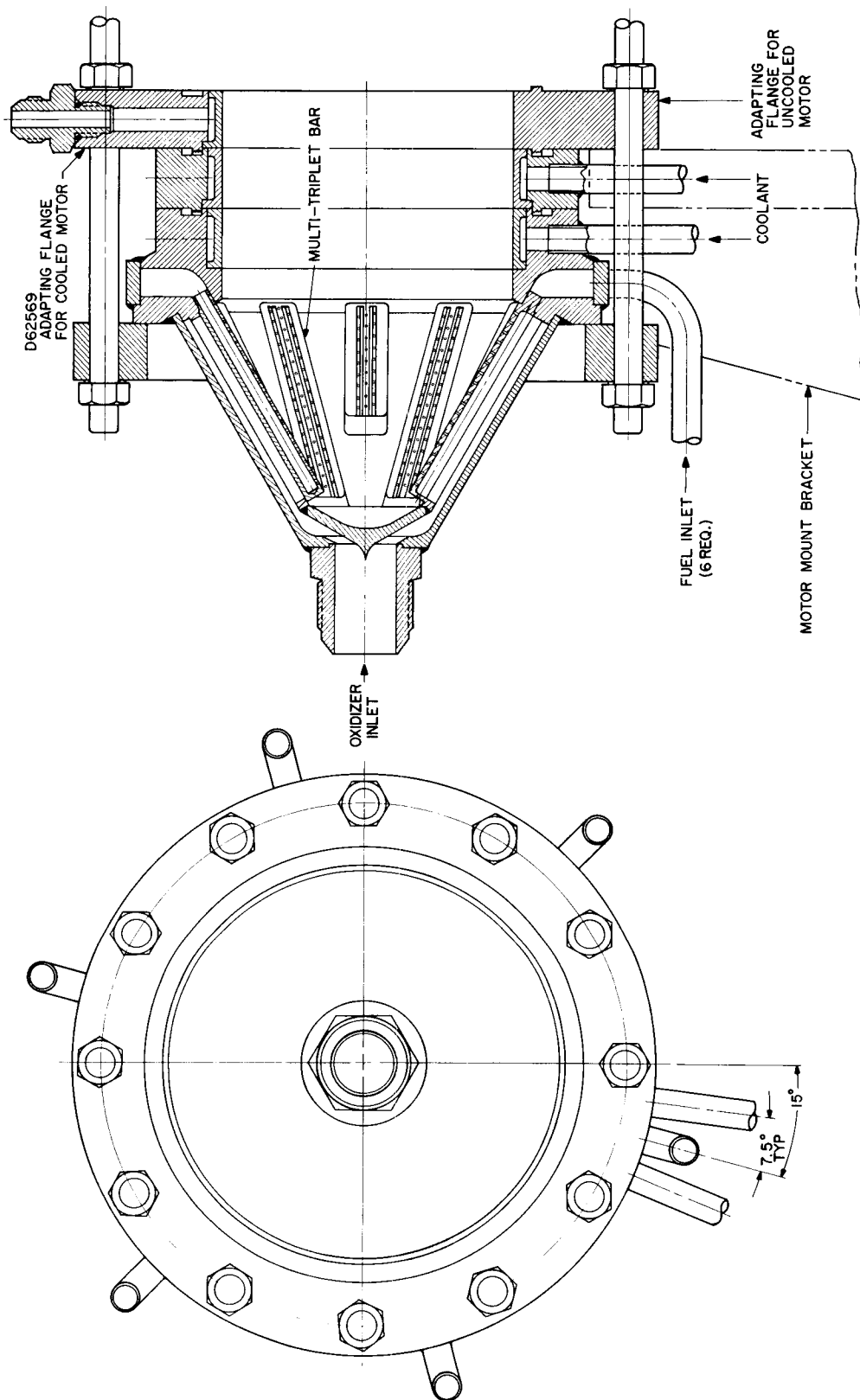
Fig. A-9. Conical shell-multitriplet injector

the triplet fans, while parallel, did not impinge edgewise on each other.

There was a total of 162 triplet elements distributed in linear arrays on the back-cone of the injector. Good mixing was anticipated from:

1. Impingement of the streams at the small individual triplet elements

2. Interaction between adjacent triplet fans

3. Interaction between downstream triplet fans and hot combustion gases from propellant injected at the triplets nearer the apex of the cone

In operation this injection burned out after four tests, and the initial tests had low performance. It appeared that the linear concentrations of propellant caused by injection through the triplet bar-arrays had induced circulating currents of hot combustion products which eroded the injector elements.

VI. CYLINDRICAL CUP MULTI-ELEMENT INJECTOR

Previous injectors had used fairly large propellant streams or had introduced the propellant in the form of a spray or a sheet in a small portion of the cross-sectional area of the combustion chamber. This injector was designed to introduce the propellant with as uniform as possible a distribution throughout the cross section of the combustion chamber. In this way, the formation of large circulating eddies of hot gas and combustion products could be avoided, and heat transfer and erosion problems in the combustion chamber could be lessened.

Injection was from 14 cylindrical cup elements distributed across the face of the injector. Within each element, eight streams of each propellant component impinged against the inside wall of the element and splashed sideways to mix with the splash from the adjacent stream of the other propellant component (Fig. A-10, A-11, A-12). The propellant emerged in a predominantly axial direction.

This injector incorporated the features and advantages listed for the final multi-element injector in the main text of this report. Reasonably good performance was obtained, but after several tests, attack and erosion were evident on the insides of the element cups. Figure A-13 shows the culmination of this erosion. It was evident that the mixing and reaction of the propellants on the surface of the cup generated temperatures which made the attack possible, since the cool propellants individually did not attack other parts of the aluminum alloy injector. The cure for the erosion problem, while retaining all the other advantages of this type of injector, appeared to be to splash the propellant streams against separate metal surfaces, each of which would be bathed in, and cooled by, only one propellant, while allowing some mixing and reaction to occur in the space inside of the cup. This modification resulted in the injector which is described in the main portion of this report.
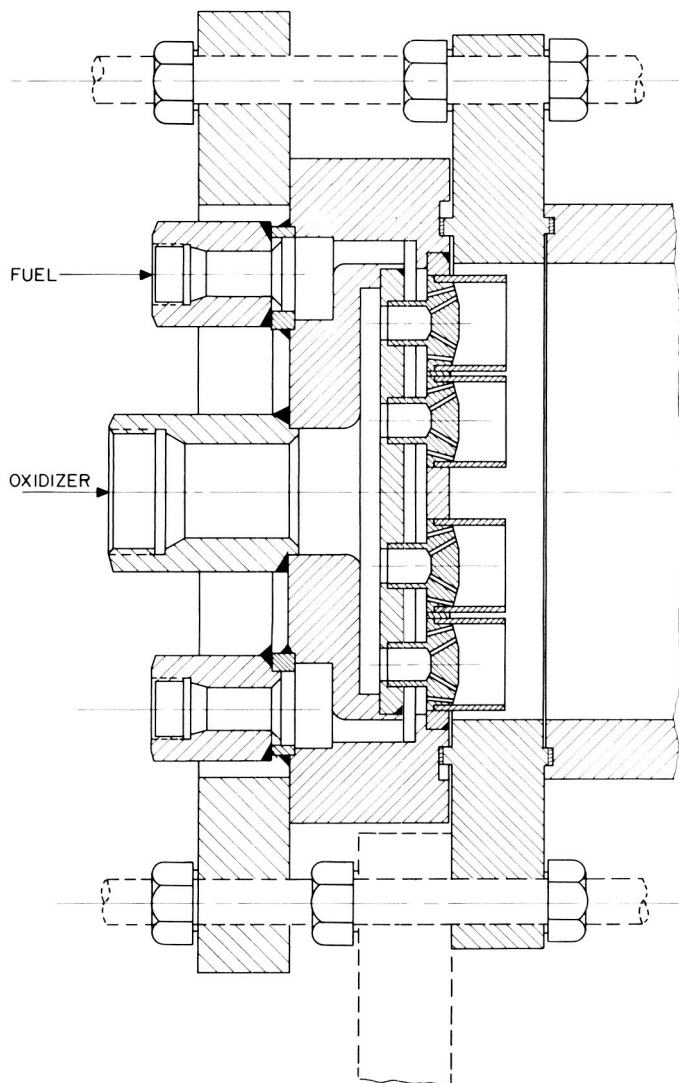
FUEL

OXIDIZER

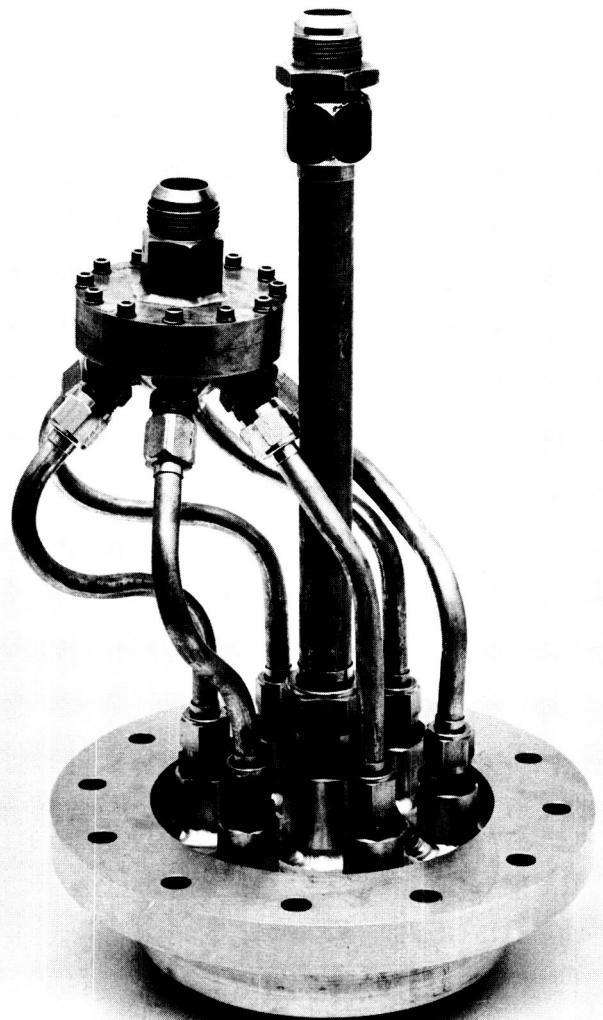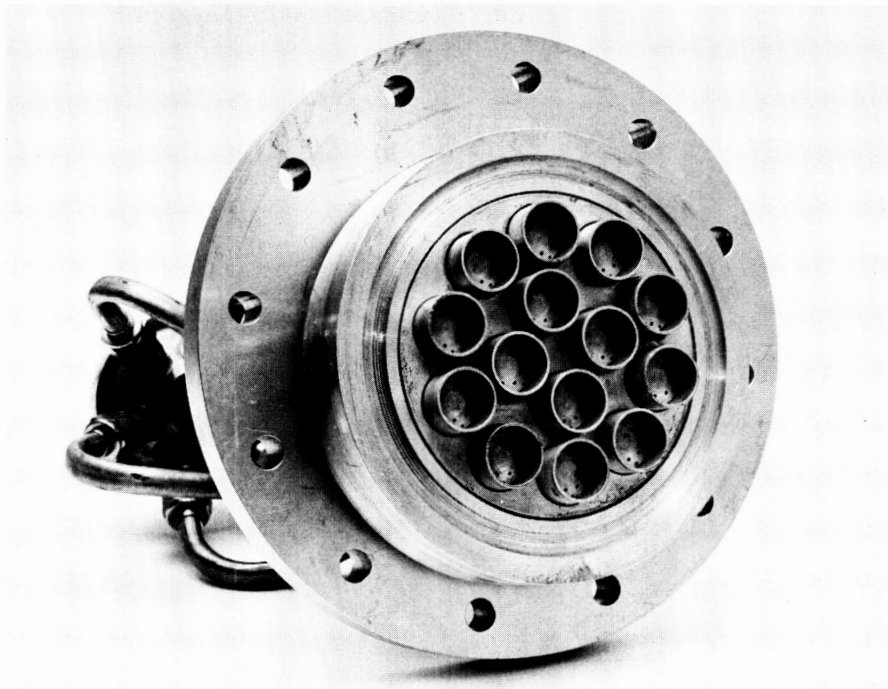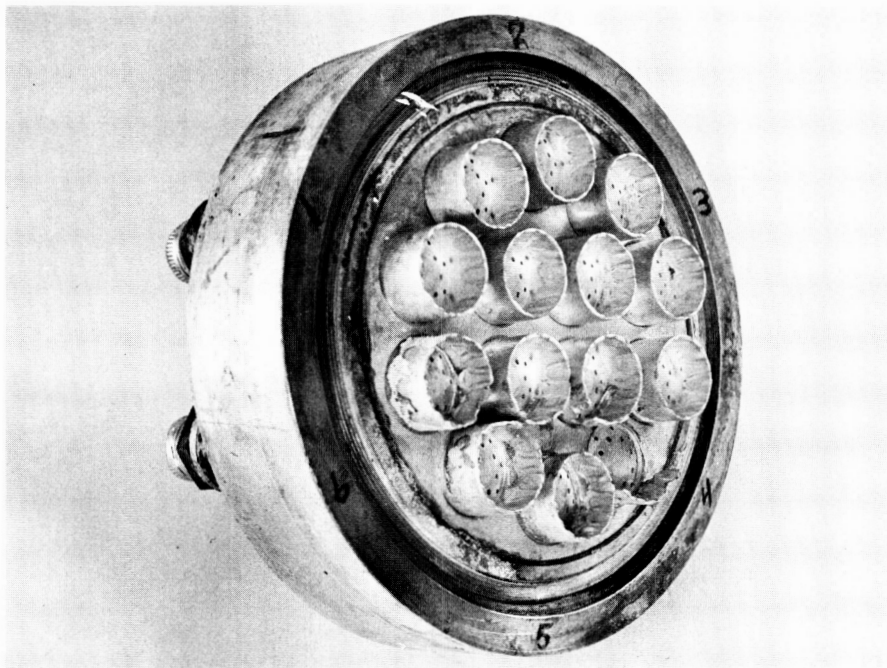**Fig. A-10. Cylindrical cup multi-element injector coupled to uncooled motor chamber**

Fig. A-11. Propellant manifolding of cylindrical cup multi-element injector

Fig. A-12. Cylindrical cup multi-element injector,
face view

Fig. A-13. Erosion of cylindrical cup multi-element
injector after many tests

APPENDIX B

Comparison of Measured and Predicted Nozzle Heat Flux

A simplified enthalpy-potential method was used to predict nozzle heat flux for comparison with the heat flux measured during four typical tests in which the water-cooled sectional nozzle was used.

The prediction method is similar to that described in Ref. 7, and is defined by the following equations:

$$q = h_i (i_o - i_w)_{exp} \qquad (B-1)$$

$$h_i = \left[\frac{0.026}{D_*^{0.20}} \left(\frac{\mu^{0.20}}{Pr^{0.60}} \right)_{0, exp} \left(\frac{p_c g}{C^*} \right)_{exp}^{0.80} \right.$$
$$\left. \times \left(\frac{D_*}{R_{c*}} \right)^{0.10} \right] \left(\frac{A_*}{A} \right)^{0.80} \sigma_{exp} \qquad (B-2)$$

$$\sigma_{exp} = \left[\left(\frac{\rho_{ref}}{\rho_s} \right)^{0.80} \left(\frac{\mu_{ref}}{\mu_0} \right)^{0.20} \right]_{exp} \qquad (B-3)$$

$$T_{ref} = \left[\frac{(T_s + T_w)}{2} \right]_{exp} \qquad (B-4)$$

$$\mu = 46.6 \times 10^{-10} M^{1/2} T^{0.6} \qquad (B-5)$$

$$Pr = \frac{4\bar{\gamma}}{9\bar{\gamma} - 5} \qquad (B-6)$$

The required experimental value of the combustion gas stagnation temperature is obtained by using the experimental characteristic velocity or effective exhaust velocity, compared with the corresponding ideal equilibrium value of characteristic velocity or exhaust velocity, to correct the ideal equilibrium temperature. Thus:

$$\eta_c \eta_q = \frac{C_D \left(\frac{p_c A_* g}{w} \right)_{exp}}{c_{ideal}^*} \simeq \frac{\left(\frac{Fg}{w} \right)_{exp}}{\lambda c_{ideal}} \qquad (B-7)$$

$$T_{o, exp} = T_{o, ideal} (\eta_c \eta_q)^2 \qquad (B-8)$$

An ideal equilibrium isentropic performance calculation for the propellant at the given mixture ratio and chamber pressure, having the stagnation temperature fixed at $T_{o, exp}$, is used to obtain corresponding values for i_o, $\bar{M}$, γ, c^*, and for T_s as a function of contraction or expansion area ratio. For the present heat-transfer comparison, the wall temperature of the water-cooled copper nozzle was assumed to be constant at 350°F, and the enthalpy, i_w, of the equilibrium products of combustion at this temperature was obtained from the computer program used for the performance calculation with fixed initial stagnation temperature.

A comparison of measured and predicted nozzle heat transfer is shown on Figs. 16, 19, 22, and 23. In Figs. 19, 22 and 23 the predicted heat flux is low in the region upstream of the throat and at the throat itself. In the diverging section of the nozzle, the agreement is reasonably good, with the predicted heat flux being only slightly higher than the measured heat flux.

The predicted heat flux corresponding to the test shown in Fig. 16 is close to that of the other similar tests, but in this instance the measured heat flux in the throat and downstream nozzle regions is unaccountably lower than that measured during the other tests. All other test data, (Figs. 17 through 23), indicate higher heat flux at the throat and in the diverging section of the nozzle than that shown in Fig. 16. Therefore, it is presumed that Figs. 19, 22 and 23 indicate the most probable relationship between measured and predicted heat flux over the range of motor operating conditions covered by these tests.

In Ref. 7 it is shown that the agreement between predicted and measured nozzle heat flux varies with changes in chamber pressure and in chamber-to-nozzle contraction area ratio, as well as with changes in injector configuration. The comparison between test data and analytical prediction in Figs. 16, 19, 22 and 23 lie well within the range covered by the comparisons of Ref. 7.

It should be emphasized that the prediction formula used here is a modified form of a correlation for a convective heat-transfer process. It has been found useful for approximate prediction of rocket motor nozzle heat transfer in the ranges of chamber pressure and contraction area ratio which are in common use. Equations (B-1) through (B-4) should not be used outside the region of known applicability without further investigation.

NOMENCLATURE FOR APPENDIX B

A_* throat area

C_D nozzle discharge coefficient

D_* throat diameter

$\overline{M}$ average molecular weight

Pr Prandtl number

$R_{c,*}$ radius of curvature of nozzle throat

T_0 stagnation temperature

T_s static temperature

T_w wall temperature

h_i heat-transfer coefficient, enthalpy[1]

i_0 stagnation enthalpy

i_w enthalpy of combustion products in equilibrium at wall temperature

q heat flux

$\eta_c\eta_q$ performance correction factor for combustion inefficiency and heat loss

$\overline{\gamma}$ ratio of specific heats, mean

λ momentum loss coefficient due to nozzle divergence

ρ density

μ viscosity[2]

Subscripts

$_0$ stagnation condition value

$_{exp}$ experimental condition value

$_w$ propellant flow rate

---

(1) h_i is in lbm/in.^{2} sec when D_* is in inches, μ is in lbm/in. sec, and $p_c g/c^*$ is in lbm/in.^{2} sec. (Eq. B-2).

(2) μ is in lbm/in. sec when T_0 is in °R (Eq. B-5).

REFERENCES

1. Jet Propulsion Laboratory, *Combined Bimonthly Summary No. 56,* for period October 1 to December 1, 1956 (Confidential), Jet Propulsion Laboratory, Pasadena, Calif.

2. Allied Chemical and Dye Corp., "Chlorine Trifluoride and Other Halogen Fluorides," Technical Bulletin TA-8532-2, Allied Chemical and Dye Corp., General Chemical Div., New York, N. Y.

3. Battelle Memorial Institute, Liquid Propellants Handbook, Battelle Memorial Institute, Columbus, Ohio, October 31, 1955.

4. Jet Propulsion Laboratory, *Combined Bimonthly Summary No. 67,* for the period August 1 to October 1, 1958 (Confidential), Jet Propulsion Laboratory, Pasadena, Calif.

5. Powell, W. B., Howell, G. W., Irving, J. P., "A Method for the Determination of Local Transient Heat Flux in Uncooled Rocket Motors," Technical Report No. 32-257, Jet Propulsion Laboratory, Pasadena, Calif., July 1962.

6. *Journal of Scientific Instruments,* Vol. 37, p. 221, June 1960.

7. Welsh, W. E., Jr., and Witte, A. B. "A Comparison of Analytical and Experimental Local Heat Fluxes in Liquid-Propellant Rock Thrust Chambers." Technical Report 32-43, Jet Propulsion Laboratory, Pasadena, February 1, 1961.